



**HAL**  
open science

# Design of Multirotor Aerial Vehicles: a Taxonomy Based on Input Allocation

Mahmoud Hamandi, Federico Usai, Quentin Sablé, Nicolas Staub, Marco Tognon, Antonio Franchi

## ► To cite this version:

Mahmoud Hamandi, Federico Usai, Quentin Sablé, Nicolas Staub, Marco Tognon, et al.. Design of Multirotor Aerial Vehicles: a Taxonomy Based on Input Allocation. 2020. hal-02433405v1

**HAL Id: hal-02433405**

**<https://hal.science/hal-02433405v1>**

Preprint submitted on 9 Jan 2020 (v1), last revised 21 May 2021 (v2)

**HAL** is a multi-disciplinary open access archive for the deposit and dissemination of scientific research documents, whether they are published or not. The documents may come from teaching and research institutions in France or abroad, or from public or private research centers.

L'archive ouverte pluridisciplinaire **HAL**, est destinée au dépôt et à la diffusion de documents scientifiques de niveau recherche, publiés ou non, émanant des établissements d'enseignement et de recherche français ou étrangers, des laboratoires publics ou privés.

# Survey on Aerial Multirotor Design: a Taxonomy Based on Input Allocation

Mahmoud Hamandi, Federico Usai, Quentin Sable, Nicolas Staub, Marco Tognon and Antonio Franchi

**Abstract**—This paper reviews the impact of *multirotor aerial vehicles* designs on their abilities in terms of tasks and system properties. We propose a general taxonomy to characterize and describe multirotor aerial vehicles and their design, which we apply exhaustively on the vast literature available. Thanks to the systematic characterization of the designs we exhibit groups of designs having the same abilities in terms of achievable tasks and system properties. In particular, we organize the literature review based on the number of *atomic actuation units* and we discuss global properties arising from their choice and spatial distribution in the designs. Finally, we provide a discussion on the common traits of the designs found in the literature and the main future open problems.

## I. INTRODUCTION

The study of *unmanned aerial vehicles* (UAVs) has been widely investigated in the last decades, leading to several well-known applications. In particular, the topic of micro multirotors yielded to several scientific results in the fields of path planning and control theory, as well as localization and mapping.

These results and their corollary commercial applications are highly based on a single multirotor design: the *coplanar/collinear propeller design* (with 4, 6, 8 propellers). In this design, the propeller centers are all placed on the same plane (coplanar) and their angular velocities are collinear, *i.e.*, their produced thrusts are all oriented in the same direction. This design is favored for its mechanical simplicity, energetic efficiency, and its hovering capability, which makes it a good candidate for applications such as visual inspection, survey, and mapping. The system abilities and properties for *coplanar/collinear multirotors* are widely understood in the community, thanks to the vast literature, which comprises well-publicized quad-, hexa- and octo-rotors, as well as original designs like the reconfigurable flying array presented in (Oung et al. 2010) and snake-like designs as in (Zhao et al. 2017; Anzai et al. 2017).

In the last decade, several researchers explored multiple designs of multirotors to overcome some limitations of coplanar/collinear designs. Hobby-racers' quest for fast and agile maneuvers led to the exploration of designs allowing more yaw control authority, such as tri-rotors and Vtail quadrotors. Similarly, works focused on physical interaction and manipulation led to a large variety of alternative multirotor designs

aimed at applying forces and moments to the environments. Design-oriented papers aimed at improving existing designs by adding propellers, increasing thrust-vectoring, or optimizing the propeller position and orientation in the body of the platform to accomplish specific tasks. However, a rigorous classification of such new designs and a comparison of their properties has not yet been addressed in the literature.

This paper aims at presenting an exhaustive and up-to-date review of the vast variety of multirotor designs proposed by the academic and industrial communities in recent years, with an emphasis on the properties and abilities of each platform. The platforms are ordered in classes of designs revolving around the number, nature, and placement of *actuation units*, which are pivotal in defining the motion and interaction capabilities of the platform. We propose a rigorous classification of the designs based on the resulting force/moment allocation property, and we show the relation between such allocation property and the task abilities of the platforms. In this way, it is natural for the reader to understand what a given platform is capable of. At the same time, the question of which design possesses a given property is provided in an extensive set of summarizing tables across the paper. For a complete understanding of these tables, we provide a summary of all the abbreviations and symbols in Tab. I. The rest of the paper is organized as follows, the first section provides the required definitions to structure the discussion, as well as the modeling of generic multirotor design. The second part of the paper groups the analysis of different designs based on the number of motors generating thrust. The main findings and generalities that can be extracted from the review are then summarized in the discussion section. Lastly, the conclusion section concludes the paper.

## II. DEFINITIONS AND CONVENTIONS

### A. Review Scope

In this paper, we focus our analysis on multirotors, *i.e.*, rotary-wing vehicles, for which the control inputs are solely the spinning velocities of each propeller and, possibly, the propeller orientation. This scope excludes UAV designs where propellers are mixed with wings in which the control input also comprises the wing geometry, *i.e.*, designs in which a subsequent part of the lift is generated by fixed-wing. Some examples are (Bronz et al. 2017) or the hybrid designs reviewed in (Saeed et al. 2015). The scope of this manuscript also excludes multirotors with variable pitch propeller mechanisms, where the propeller pitch is a control input rather than, or in addition to, the propeller speed, *e.g.*, the quadrotor based design in (Michini et al. 2011). Designs in which the motion

All the authors are with LAAS-CNRS, Université de Toulouse, CNRS, Toulouse, France, mahmoud.hamandi@laas.fr, marco.tognon@laas.fr, quentin.sable@laas.fr, antonio.franchi@laas.fr

Antonio Franchi is also with the Robotics and Mechatronics lab, Faculty of Electrical Engineering, Mathematics & Computer Science, University of Twente, Enschede, The Netherlands a.franchi@utwente.nl.

entry	explanation
apparition	Lists the reference(s) of the paper(s) explaining this design
$n_u$	Represents the number of actuation controls, including the number of thrusters $N$ in addition to the number of servomotor control inputs
DoF	Shows which propeller tilt angles are actuated; entries between parenthesis represent angles that are driven synchronously, <i>i.e.</i> , constitute one control input
properties	Lists the possible actuation properties for this design as detailed in System Properties
abilities	Lists the level of all the abilities for this design as detailed in System Abilities
maturity	Maturity of the design presented in the apparition paper(s)
variant of figure	The closest figure representing this design

TABLE I: This table summarizes the expected entry in each column of the recapitulative tables shown throughout the paper. Note that each table corresponds to platforms with a specific number of AAU noted as  $N$ .

of weights is used as control input are also excluded, as, *e.g.*, the quadrotor based design in (Haus et al. 2016). Additionally, designs in which the multirotor center of mass (CoM) is time varying are also out of the scope of this paper. This includes some of the previously mentioned cases but also designs where weight motion participate in the system stabilization. Examples of such stabilization systems can be found in (Haus et al. 2017), and in (Zhao et al. 2017; Anzai et al. 2017). Nevertheless, to accommodate for manufacturing imperfections and mechanical constraints, we consider the non-moving CoM in a relaxed way, allowing small displacement of the CoM due to the motion of the actuators. Lastly, designs where the weight is partially or totally lifted by means other than the rotating propellers are also excluded. This category includes for example platforms lifted through a gas such as helium or ropes, similar to the design presented in (KG 2016; Sarkisov et al. 2019).

Consequently, the considered designs include the control quantities related to: i) the spinning propellers, each producing mainly a thrust (a lift) and a drag moment, and possibly ii) the vectorization of their orientation in the body frame.

## B. Design Framework

Under the previous assumptions, to describe the various possible designs of small multirotors, we propose a general abstract framework defined as follows.

*Definition 1:* A multirotor design is considered as a rigid body, made of fixed mechanical elements, to which some *Atomic Actuation Units* (AAUs) are attached. The design so defined is completely described by:

- 1) the number of AAUs, denoted by  $N \in \mathbb{N}_{>0}$ ,
- 2) the type of every single AAU, and
- 3) spatial distribution of the AAUs.

For the sake of classifying multirotor platforms according to the properties related to their actuation (*actuation properties*), we consider here only the design parameters directly linked to the vehicle actuation. On the other hand, we do not consider design parameters like total weight, flight electronics, power source, materials, the shape of the structure and so on. Although very important for the final development of an aerial platform, those parameters are tailored by the particular

	Central body
	Joint
	Possibly independently actuated joint
	Counter clockwise (CCW) rotating propeller
	Clockwise (CW) rotating propeller
	Body with a non-tiltable propeller
	Body with a propeller tiltable radially (angle $\alpha$ )
	Body with a propeller tiltable tangentially (angle $\beta$ )
	Body with a propeller tiltable in $S^2$ (both angles $\alpha$ and $\beta$ )
	Gears indicating a coupling in the tilting of the corresponding joints

TABLE II: Overview of platform design components. This table summarizes the different components used to design a platform. The different component representations are used hereafter to visualize platform designs.

application and do not grant the platform particular properties of interest for this study.

*Remark 1:* In Tab. II we summarize the considered body parts that affect the actuation properties of interest. We shall use these elements as a standard to highlight the main actuation elements and graphically visualize the actuation characteristics of each platform. For each of them, we shall provide a

conceptual design representation made of the body parts of Tab. II.

We denote by  $\mathcal{B}$  the body frame rigidly attached to the multirotor. Its origin  $O_B$  coincides with the rigid body CoM and its main axes are denoted by  $\mathbf{x}_B, \mathbf{y}_B, \mathbf{z}_B$ , respectively.

*Actuation Units – AAUs:* are the mechatronic components generating thrust. They are the core of each multirotor design. In the literature, they typically consist of a brushless motor with a single propeller.

Considering a generic  $i$ -th AAU, we denote by  $w_i \in \mathbb{R}$  the *propeller spinning rate* and by<sup>1</sup>  $\mathbf{v}_i \in \mathbb{S}^2$  the coordinates of the *spinning axis* expressed in  $\mathcal{B}$ .

Besides, we define a frame  $\mathcal{F}_{P_i}$  rigidly attached to the  $i$ -th AAU, with origin  $O_{P_i}$  coinciding with the CoM of the  $i$ -th AAU, and with axes  $\mathbf{x}_{P_i}, \mathbf{y}_{P_i}, \mathbf{z}_{P_i}$  such that  $\mathbf{z}_{P_i}$  is the spinning axis and  $\mathbf{y}_{P_i}$  is perpendicular to both  $\overline{O_B O_{P_i}}$  and  $\mathbf{z}_{P_i}$ . The position of  $O_{P_i}$  w.r.t.  $\mathcal{B}$  is given by the vector  ${}^B \mathbf{p}_i \in \mathbb{R}^3$ .

It is convenient to parametrize  $\mathbf{v}_i$  using two angles  $\alpha_i$  and  $\beta_i$  which are defined as follows:

- $\alpha_i$  is the angle needed for a rotation about  $\overline{O_B O_{P_i}}$  to bring  $\mathbf{z}_B$  into a vector  $\mathbf{z}'_B$  contained in the plane spanned by  $\overline{O_B O_{P_i}}$  and  $\mathbf{z}_{P_i}$
- $\beta_i$  the angle needed for a rotation about the axis perpendicular to the plane spanned by  $\overline{O_B O_{P_i}}$  and  $\mathbf{z}_{P_i}$  to let  $\mathbf{z}'_B$  coincide with  $\mathbf{z}_{P_i}$ .

These two rotations can be combined into a single rotation matrix<sup>2</sup>  ${}^B \mathbf{R}_{P_i} \in SO(3)$  defined as  ${}^B \mathbf{R}_{P_i} = \mathbf{R}_2(\beta_i) \mathbf{R}_1(\alpha_i)$  where  $\mathbf{R}_1(\alpha_i)$  and  $\mathbf{R}_2(\beta_i)$  are the two aforementioned rotations, thus obtaining  $\mathbf{v}_i = {}^B \mathbf{R}_{P_i} \mathbf{e}_3$ , where  $\mathbf{e}_3 = [0 \ 0 \ 1]^T$ . Notice that such rotations are the one performed by the two servomotors depicted in Table II. Furthermore, notice that this parametrization is valid as long as  $\overline{O_B O_{P_i}}$  and  $\mathbf{z}_{P_i}$  are not parallel.

The propeller rotation produces a thrust  $\mathbf{f}_i \in \mathbb{R}^3$ , and a drag moment  $\mathbf{m}_i \in \mathbb{R}^3$ . This force and moment pair can be expressed w.r.t. the CoM of each corresponding propeller as follows:

$$\begin{aligned} \mathbf{f}_{P_i} &= c_{f_i} |w_i| w_i \mathbf{v}_i \\ \mathbf{m}_{P_i} &= k_i c_{\tau_i} |w_i| w_i \mathbf{v}_i, \end{aligned} \quad (1)$$

where  $c_{f_i} \in \mathbb{R}_{>0}$  and  $c_{\tau_i} \in \mathbb{R}_{>0}$  are positive constants whose value depends on the shape of the corresponding propeller. The term  $k_i \in \{-1, 1\}$  accounts for the direction of rotation of the propeller w.r.t.  $\mathbf{v}_i$ . As such,  $k_i = -1$  (or  $k_i = 1$ ) if the thrust has the same (or the opposite) direction of  $\mathbf{v}_i$ , and the propeller is consequently considered of CCW (or CW) type.

As normally done in the related literature, in (1) we neglected all the secondary inertia and aerodynamic effects, like centripetal and flapping effects, see (R. Mahony et al. 2012). In fact, in the considered working conditions, these are negligible w.r.t. the main thrust and drag moment contributions.

Assuming that the brushless motor can control  $w_i$ , we can define  $u_{\lambda_i} = |w_i| w_i \in \mathbb{U}_{\lambda_i} \subset \mathbb{R}$  as one of the controllable inputs for the  $i$ -th AAU. In particular, this is the input that

<sup>1</sup> $\mathbb{S}^n = \{\mathbf{x} \in \mathbb{R}^{n+1} \mid \|\mathbf{x}\| = 1\}$   
<sup>2</sup> $SO(3) = \{\mathbf{R} \in \mathbb{R}^{3 \times 3} \mid \mathbf{R}^T \mathbf{R} = \mathbf{I}_3, \det(\mathbf{R}) = 1\}$ , where  $\mathbf{I}_i \in \mathbb{R}^{i \times i}$  is the identity matrix of dimension  $i$ .

AAU key param.	Short descrip.	Influence
Aerodynamic param.	Propeller shape	Thrust/drag coefficient
Uni or bidirectional thrust	$w_i > 0$ or $w_i < 0$	Thrust and drag direction
Fixed or actuated spinning axis	$\alpha$ fixed or actuated $\beta$ fixed or actuated	Thrust vectoring
Position of $O_{P_i}$	${}^B \mathbf{p}_i$	Moment generation

TABLE III: Impact of the AAUs key parameters.

controls the intensity of the produced force and moment. The equations in (1) can be rewritten w.r.t.  $\mathcal{B}$ , with the addition of the force-induced moments as follows:

$$\begin{aligned} \mathbf{f}_i &= c_{f_i} \mathbf{v}_i u_{\lambda_i} \\ \mathbf{m}_i &= k_i c_{\tau_i} \mathbf{v}_i u_{\lambda_i} + {}^B \mathbf{p}_i \times \mathbf{f}_i. \end{aligned} \quad (2)$$

The parameters required to characterize AAUs are:

1) *Aerodynamic parameters.* The shape of the propeller is an important design factor that defines the lift and drag coefficients, i.e.,  $c_{f_i}$  and  $c_{\tau_i}$ , respectively. Those aerodynamic parameters impact the maximum payload and the energy consumption of the vehicle. According to the particular task, the propeller design should be optimized to meet the particular requirements.

2) *Unidirectional or bidirectional thrust.*

The second key parameter to consider is the direction of the thrust along the spinning axis. In general, brushless motor controllers can rotate the propeller only in one direction, i.e.,  $0 \leq \underline{w}_i \leq w_i \leq \bar{w}_i$  where  $\underline{w}_i, \bar{w}_i \in \mathbb{R}_{\geq 0}$ , making the thrust *unidirectional*. Nevertheless, for some designs with particular brushless motor controllers and propeller profile, as in (Brescianini and D'Andrea 2016), the propellers can spin in both directions. In this case  $\underline{w}_i \leq w_i \leq \bar{w}_i$  where  $\underline{w}_i \in \mathbb{R}_{<0}$  and  $\bar{w}_i \in \mathbb{R}_{>0}$ , making the thrust *bidirectional*.

Although this solution enlarges the thrust range, it usually results in a lower thrust magnitude w.r.t. to uni-directional propeller for the same spinning velocity. In fact, it requires propeller designs that are flat enough to generate thrust in both directions in the same way.

3) *Fixed or actuated spinning axis.* The third key parameter to consider for each AAU is its ability to re-orient its thrust, either actively or passively. In this case we have that

$$\mathbf{v}_i = f_{\mathbf{v}_i}(\mathbf{u}_{\mathbf{V}}), \quad (3)$$

where  $f_i : \mathbb{R}^m \rightarrow \mathbb{S}^2$  and  $\mathbf{u}_{\mathbf{V}} = [u_1^T \dots u_m^T]^T \in \mathbb{U}_{\mathbf{V}} = \times_{j=1}^m \mathbb{U}_{\mathbf{v}_j} \subset \mathbb{R}^m$  gathers the angular positions of the shafts of the servo motors that control the orientation of the spinning axis, where we noted by  $m \leq 2N$  the number of servomotors.

This property can be used to change the vectoring direction of the total thrust produced by the combination of all AAUs without changing their spinning velocities.

In what follows, we consider  $\mathbf{u}_{\mathbf{V}}$  as a state due to its slower dynamics relative to the applied thrust. Instead, we consider its derivative  $\dot{\mathbf{u}}_{\mathbf{V}}$  as the entity controlled by the  $m$  servo motors, thus the real input. We can write the dynamic extension of (3):

$$\dot{\mathbf{v}}_i = \frac{d\mathbf{v}_i}{dt} = \frac{\partial f_{\mathbf{v}_i}}{\partial \mathbf{u}_{\mathbf{V}}} \dot{\mathbf{u}}_{\mathbf{V}}. \quad (4)$$

UAV	Unmanned Aerial Vehicle
AAU	Atomic Actuation Unit
ESC	Electronic Speed Control
UDT	Uni-Directional Thrust
MDT	Multi-Directional Thrust
FA	Fully Actuated
OA	Over Actuated
OD	Omni Directional
$\mathbf{F}$	Full Allocation Matrix
$N$	Number of AAUs in a platform
$n_u$	Number of control inputs throughout the paper, it is listed as $n_u = n_\lambda + m$
$n_\lambda$	Number of thrust input controls
$m$	Number of thrust-vectoring input controls
$\mathbb{U}$	Input control space
$\mathbf{v}_i$	Spinning axis of $i$ -th AAU
$\alpha_i$	Radial tilting angle of $i$ -th propeller
$\beta_i$	Tangential tilting angle of $i$ -th propeller
$\mathcal{F}_1$	Image of the force space on the domain $\mathbb{U}$ subject to zero moment

TABLE IV: This table summarizes the main abbreviations used in the paper and lists useful mathematical notations.

4) *Position of  $O_{P_i}$* . Finally, the fourth key parameter to consider for each AAU is its position w.r.t.  $O_B$ . In fact,  ${}^B\mathbf{p}_i$  affects the total moment applied on the CoM of the platform as shown in (2).

Table III gathers the previously mentioned parameters and their effects on the produced total thrust and moment. Table IV summarizes the main abbreviations and notations used in this section and the rest of this paper.

### C. Platform Equations of Motion

Let us consider a world frame  $\mathcal{W}$ , centered in  $O_W$  and such that it follows the East-North-Up (ENU) convention. Its main axes are denoted  $\mathbf{x}_W, \mathbf{y}_W, \mathbf{z}_W$  respectively.

Considering the body frame  $\mathcal{B}$  previously defined, its position and the orientation w.r.t.  $\mathcal{W}$  are denoted with  ${}^W\mathbf{p}_B \in \mathbb{R}^3$  and  ${}^W\mathbf{R}_B \in \text{SO}(3)$ , respectively. To fully describe the state of the vehicle, we also define the linear velocity of the origin of  $\mathcal{B}$  by the vector  ${}^B\dot{\mathbf{p}}_B \in \mathbb{R}^3$ , and its angular velocity w.r.t.  $\mathcal{W}$  by the vector  ${}^B\boldsymbol{\omega}_B \in \mathbb{R}^3$ , both expressed in  $\mathcal{B}$ .

For the sake of compactness, we introduce the following notations. Let  ${}^B\mathbf{P} = [{}^B\mathbf{p}_1 \dots {}^B\mathbf{p}_N] \in \mathbb{R}^{3 \times N}$  and  $\mathbf{V} = [\mathbf{v}_1 \dots \mathbf{v}_N] \in \mathbb{R}^{3 \times N}$  be the concatenation matrices of all AAUs positions and spinning axes, respectively. We define the time derivative of  $\mathbf{V}$  as  $\dot{\mathbf{V}} = [\dot{\mathbf{v}}_1 \dots \dot{\mathbf{v}}_N] \in \mathbb{R}^{3 \times N}$ . We also denote by  $\mathbf{u}_\lambda = [u_{\lambda_1} \dots u_{\lambda_N}]^T \in \mathbb{U}_\lambda \subset \mathbb{R}^{n_\lambda}$  the vector gathering the control inputs relative to the thrust intensity. Notice that  $\mathbb{U}_\lambda = \times_{i=1}^N \mathbb{U}_{\lambda_i}$ ,  $n_\lambda = N$ . The total control input vector is denoted by  $\mathbf{u} = [\mathbf{u}_\lambda^T \ \mathbf{u}_V^T]^T \in \mathbb{U} \subset \mathbb{R}^{n_u}$  and  $\mathbb{U} = \mathbb{U}_\lambda \times \mathbb{U}_V$  denotes the set of feasible inputs. Notice that, if the orientation of all the AAUs is fixed, *i.e.*, not actuated, then  $\mathbf{u} = \mathbf{u}_\lambda$  and  $n_u = n_\lambda$ .

Let us define  $\mathbf{w} \in \mathbb{R}^6$  as the actuation wrench applied to the platform, and  $\mathbb{W}$  as the set of feasible wrenches. Following (2), we can write

$$\mathbf{w}(\mathbf{u}) = \begin{bmatrix} \mathbf{f}(\mathbf{u}) \\ \mathbf{w}(\mathbf{u}) \end{bmatrix} = \sum_{i=1}^N \begin{bmatrix} \mathbf{f}_i(\mathbf{u}) \\ \mathbf{m}_i(\mathbf{u}) \end{bmatrix}. \quad (5)$$

To characterize  $\mathbf{w}$ , and in particular how an input variation affects  $\mathbf{w}$ , we introduce the *full allocation matrix*  $\mathbf{F} \in \mathbb{R}^{6 \times n_\lambda}$  defined as:

$$\mathbf{F}(\mathbf{u}_V) = \frac{\partial \mathbf{w}}{\partial \mathbf{u}} = \begin{bmatrix} \frac{\partial \mathbf{f}}{\partial \mathbf{u}_\lambda}(\mathbf{u}_V) & \frac{\partial \mathbf{f}}{\partial \mathbf{u}_V}(\mathbf{u}_V) \\ \frac{\partial \mathbf{m}}{\partial \mathbf{u}_\lambda}(\mathbf{u}_V) & \frac{\partial \mathbf{m}}{\partial \mathbf{u}_V}(\mathbf{u}_V) \end{bmatrix} = \begin{bmatrix} \mathbf{F}_1(\mathbf{u}_V) \\ \mathbf{F}_2(\mathbf{u}_V) \end{bmatrix}. \quad (6)$$

We decompose  $\mathbf{F}$  into  $\mathbf{F}_1 = \partial \mathbf{f} / \partial \mathbf{u} \in \mathbb{R}^{3 \times n_\lambda}$ , and  $\mathbf{F}_2 = \partial \mathbf{m} / \partial \mathbf{u} \in \mathbb{R}^{3 \times n_\lambda}$  referred to as the *force allocation matrix* and the *moment allocation matrix* respectively.

Notice that, since the entries of  $\mathbf{u}_\lambda$  appear linearly in (2),  $\mathbf{F}$  depends only on  $\mathbf{u}_V$ .

In the case of a platform possessing only *fixed* AAU,  $\partial \mathbf{w} / \partial \mathbf{u}_V = \mathbf{0}$ , and the *full allocation matrix* is constant and can be written as

$$\mathbf{F} = \frac{\partial \mathbf{w}}{\partial \mathbf{u}} = \begin{bmatrix} \frac{\partial \mathbf{f}}{\partial \mathbf{u}_\lambda} \\ \frac{\partial \mathbf{m}}{\partial \mathbf{u}_\lambda} \end{bmatrix}. \quad (7)$$

Following the Newton-Euler formalism, the *full allocation matrix* can be made directly visible in the dynamical equation of a multirotor with fixed propellers as shown below:

$$\begin{bmatrix} m {}^B\ddot{\mathbf{p}}_B \\ \mathbf{J}^B \dot{\boldsymbol{\omega}}_B \end{bmatrix} = - \begin{bmatrix} mg {}^W \mathbf{R}_B^T \mathbf{e}_3 \\ {}^B \boldsymbol{\omega}_B \times \mathbf{J}^B \boldsymbol{\omega}_B \end{bmatrix} + \mathbf{F} \mathbf{u}_\lambda, \quad (8)$$

where  $m \in \mathbb{R}_{>0}$  and  $\mathbf{J} \in \mathbb{R}_{>0}^{3 \times 3}$  are the total mass and the positive definite inertia matrix w.r.t.  $\mathcal{B}$  of the flying system, and  $g$  is the gravitational acceleration constant.

On the other hand, in the case of a platform possessing at least one *orientable* AAU, we have to differentiate (8) to make the full allocation matrix appear:

$$\begin{bmatrix} m {}^W \ddot{\mathbf{p}}_B \\ \mathbf{J}^B \ddot{\boldsymbol{\omega}}_B \end{bmatrix} = \mathbf{g}({}^W \mathbf{p}_B, {}^W \dot{\mathbf{p}}_B, {}^W \mathbf{R}_B, \boldsymbol{\omega}_B, {}^B \mathbf{P}, \mathbf{u}_V) + \mathbf{F}(\mathbf{u}_V) \dot{\mathbf{u}}, \quad (9)$$

where  $\mathbf{g}({}^W \mathbf{p}_B, {}^W \dot{\mathbf{p}}_B, {}^W \mathbf{R}_B, \boldsymbol{\omega}_B, {}^B \mathbf{P}, \mathbf{u}_V)$  gathers all the terms that do not depend on the inputs  $\dot{\mathbf{u}}$ .

Notice that the model in (8) and correspondingly in (9) is valid under the following assumptions:

- 1) motor actuators are controlled by a fast high-gain local controller, to have a negligible transient;
- 2) gyroscopic and inertial effects due to propellers and motors are considered second-order disturbances that are neglected in the model and can be compensated by the controller itself, as specified before;
- 3) aerodynamic interactions between adjacent propellers are considered negligible, and, again, left to the robustness of the feedback controller.

### D. System Properties

One of the most important characteristics of a design is the set of the admissible wrenches  $\mathbb{W}$ . In fact, this affects the controllability of the vehicle. It is noted that the characterization of  $\mathbb{W}$  can be deduced from the number of control inputs  $n_u$ , the corresponding subspace  $\mathbb{U}$ , and the *full allocation matrix*  $\mathbf{F}$ . According to the properties of  $\mathbf{F}$ , and more in general of

$\mathbb{W}$ , we can define the following classes of multirotor aerial vehicles which are explained in detail hereafter.

- 1) Uni-directional thrust (UDT)
- 2) Multi-directional thrust (MDT)
- 3) Fully actuated (FA)
- 4) Over actuated (OA)
- 5) Omnidirectional (OD).

The interactions between the properties of classes 1) to 5) are depicted in Fig. 1.

All the listed classes have properties that extend two basic properties holding for any multirotor design and listed below.

*Property 1:* The total moment can be varied in any direction of  $\mathbb{R}^3$ , *i.e.*,

$$\text{rank} \left\{ \frac{\partial \mathbf{m}}{\partial \mathbf{u}} \right\} = 3. \quad (10)$$

This means that for any multirotor design the orientation dynamics is always fully actuated.

*Property 2:* Nonzero-force and zero-moment are an interior-feasible wrench, *i.e.*,

$$\text{int}\{\mathbb{W}\} \ni \begin{bmatrix} \bar{\mathbf{f}} \\ \mathbf{0} \end{bmatrix} \neq \begin{bmatrix} \mathbf{0} \\ \mathbf{0} \end{bmatrix}. \quad (11)$$

The above two properties are sufficient for the platform to re-orient itself in the space, and apply a force in at least one direction to counteract its weight without applying any moment (in average), thus remaining in hovering at the equilibrium. These properties are enough for the platform to hover in place, or to move around while being in the near-hovering mode. However, they do not guarantee any decoupling between the moment and the desired force direction. Further properties extend these two and better characterize  $\mathbb{W}$ , which we recall is computed by mapping  $\mathbb{U}$  through the full allocation matrix  $\mathbf{F}$ . Based on the different properties we formally define the following classes.

1) *Uni-directional thrust – UDT:* This describes platforms for which the total thrust can be varied only along one direction (like, *e.g.*, in coplanar/collinear designs). This property can be expressed as

$$\text{rank} \left\{ \frac{\partial \mathbf{f}}{\partial \mathbf{u}} \right\} = 1 \text{ and } \text{rank}\{\mathbf{F}\} = 4, \quad \forall \mathbf{u} \in \mathbb{U} \quad (12)$$

2) *Multi-directional thrust – MDT:* This describes platforms for which the total thrust can be varied along more than one direction independently from the total moment (see *e.g.*, designs like (Kawasaki et al. 2015)) and can be expressed as

$$5 \leq \text{rank}\{\mathbf{F}\} \leq 6, \quad \forall \mathbf{u} \in \mathbb{U} \quad (13)$$

3) *Fully actuated – FA:* This describes a sub-class of MDT platform, for which the total thrust can be varied along all directions independently from the total moment.

$$\text{rank}\{\mathbf{F}\} = 6, \quad \forall \mathbf{u} \in \mathbb{U} \quad (14)$$

4) *Over actuated – OA:* This terminology typically describes platforms for which there are more actuation inputs,  $n_u$ , than the degrees of freedom of the system. In our proposed nomenclature we limit this definition to only designs which are already FA. This means that a multirotor is OA if the total thrust can be varied along all directions independently from the total moment and with more than one input combination, *i.e.*,

$$\text{FA and } n_u > 6 \quad (15)$$

5) *Omni directional – OD:* This describes another sub-class of FA designs, not exclusive from OA, where the total thrust can assume any value in a spherical shell independently from the total moment.

$$\text{FA and } \begin{bmatrix} \bar{\mathbf{f}} \\ \mathbf{0} \end{bmatrix} \ni \text{int}\{\mathbb{W}\} \quad \forall \bar{\mathbf{f}} \in \text{ball}_{\mathbb{R}^3}(R) / \text{ball}_{\mathbb{R}^3}(r) \quad (16)$$

for<sup>3</sup> any  $R \geq r \geq 0 \in \mathbb{R}$ .

While these properties reflect the ability of the platform to apply forces and moments in certain directions and combinations, it does not directly reflect its ability to maneuver, stabilize its position, or interact with its environment. These abilities are affected by the set of feasible control input,  $\mathbb{U}$ , and on the specific design and hardware extensions added to the platform.

*Remark 2:* Tognon and Franchi 2018 conduct a theoretical study to characterize OD multirotors with unidirectional propellers and provide algebraic conditions to reach an OD design in the generic case of  $N \geq 7$ . In particular, it has been proved that for a design with unidirectional propellers,  $N = 7$  is the minimal number of propellers to obtain OD. The authors found similarities between omnidirectional multirotors with unidirectional AAUs, called *omniplus* ( $O_+$ ), and frictionless contact grasping, (S.-Guerrero and R.-Torres 2018).

*Remark 3:* The analysis of such properties is very important for the motion control of the vehicle. In particular, if the platform is FA, then the design of the controller is straight forward. In fact, when the platform is FA, the full allocation matrix  $\mathbf{F}$  is full rank and thus invertible. This allows applying simple *static (fixed AAUs) or dynamic (orientable AAUs) feedback linearization*. In case of fixed AAUs, we can define  $\mathbf{u}_\lambda$  by the inversion of (8):

$$\mathbf{u}_\lambda = \mathbf{F}^\dagger \left( \begin{bmatrix} m^B \ddot{\mathbf{p}}_B^* \\ \mathbf{J}^B \dot{\boldsymbol{\omega}}_B^* \end{bmatrix} + \begin{bmatrix} mg^W \mathbf{R}_B^\top \mathbf{z}^W \\ {}_B \boldsymbol{\omega}_B \times \mathbf{J}^B \boldsymbol{\omega}_B \end{bmatrix} \right), \quad (17)$$

where  ${}^B \ddot{\mathbf{p}}_B^*$  and  ${}^B \dot{\boldsymbol{\omega}}_B^*$  are new virtual control inputs. The control law (17) makes the linear and angular accelerations directly controllable.

In case of orientable AAUs, we can define the dynamic input extension  $\dot{\mathbf{u}}$  by the inversion of (9):

$$\dot{\mathbf{u}} = \mathbf{F}^\dagger \left( \begin{bmatrix} m^W \ddot{\mathbf{p}}_B^* \\ \mathbf{J}^W \ddot{\boldsymbol{\omega}}_B^* \end{bmatrix} - \mathbf{g} \right), \quad (18)$$

where  ${}^W \ddot{\mathbf{p}}_B^*$  and  ${}^W \ddot{\boldsymbol{\omega}}_B^*$  are new virtual control inputs. The control law (18) makes the linear and angular jerk directly controllable.

<sup>3</sup>ball $_{\mathbb{R}^3}(R)$  for a certain  $R \in \mathbb{R}_{>0}$  is define such that given a vector  $\mathbf{x} \in \mathbb{R}^3$ ,  $\mathbf{x} \in \text{ball}_{\mathbb{R}^3}(R)$  if  $\|\mathbf{x}\| \leq R$

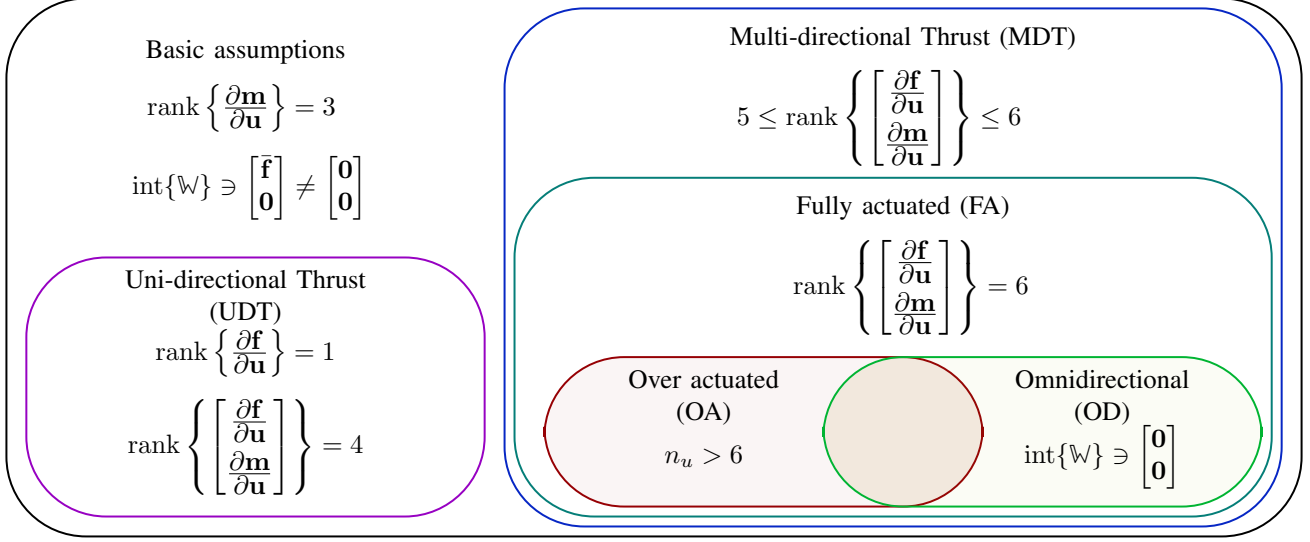


Fig. 1: interaction between thrust related properties for multirotor designs.

In both cases, the virtual inputs can be computed with a simple linear state feedback that makes  ${}^W \mathbf{p}_B^*$  and  $\omega_B^*$  stable.

If the platform is also OA, the null space of  $\mathbf{F}$  can be employed to optimize some appropriate metrics related to the inputs as done, *e.g.*, in (Ryll et al. 2015).

On the other hand, if the platform is not FA, feedback linearization cannot be directly applied, and particular attention should be dedicated to the design of the control law. As an example, for the case of a quadrotor, a first input transformation is required in order to consider as input the total thrust and moments. Afterwards, the dynamics need to be differentiated two additional times (up to the snap level) to obtain a full-rank allocation matrix, and apply feedback linearization. Notice that in this case, one needs to consider as a new input the total moment and the second derivative of the total thrust (Mistler et al. 2001).

### E. Feasible wrenches

To assess the reachable allocation capabilities of platform designs, we present throughout the paper a set of representative figures relative to the wrench space  $\mathbb{W}$ . Since this space is a 6D space which is hard to represent in 3D, we represent only the 3D projection of force space while applying zero-moment referred to as  $\mathfrak{F}_1$ . The choice of the force space with zero-moment is of particular interest for multirotors because, *e.g.*, it is important for the static hoverability analysis of the platform (Michieletto et al. 2018).

For the sake of the representation of  $\mathfrak{F}_1$ , we detail below the analysis of this space for three different cases:

*a) Case 1: Fixed propellers:* In this case, we denote by  $\mathbf{B}_2 \in \mathbb{R}^{N \times (N - \text{rank}\{\mathbf{F}_2\})}$  the basis of the null space of  $\mathbf{F}_2$ . We denote by  $\Lambda \in \mathbb{R}^{(N - \text{rank}\{\mathbf{F}_2\}) \times 1}$  as the set of points  $\lambda$  s.t.  $\mathbf{B}_2 \lambda = \mathbf{u} \in \mathbb{U}$ . Since  $\Lambda$  and  $\mathbf{u}$  are linearly related, then

the extreme points of  $\Lambda$  are the linear mapping of the extreme points of  $\mathbb{U}$  through  $\mathbf{B}_2$ . Moreover, the set  $\mathfrak{F}_1$  defined by

$$\mathbf{F}_1 \mathbf{B}_2 \lambda \quad \forall \lambda \in \Lambda \quad (19)$$

is a convex set due to the convexity of  $\mathbb{U}$ .

As such,  $\mathfrak{F}_1$  can be presented as the convex-hull of the convex set computed through (19) on the extreme points on  $\Lambda$  computed from the extreme points of  $\mathbb{U}$ .

*b) Case 2: Independently tilting propellers:* in this case, by a wise change of input coordinates, from  $\mathbf{u}$  to  $\mathbf{u}_l$ , we can transform the non-linear relation  $\mathbf{w}(\mathbf{u}) = \mathbf{F}(\mathbf{u}\mathbf{v})\mathbf{u}_\lambda$ , into a linear one  $\mathbf{w}(\mathbf{u}_l) = \mathbf{F}_l \mathbf{u}_l$ .  $\mathbf{F}_l$  and  $\mathbf{u}_l = [u_{l,1} \dots u_{l,n_u}]^\top$  are called the augmented allocation matrix and control input, respectively. Notice that  $\mathbf{F}_l$  does not depend on  $\mathbf{u}_v$ .

Considering the representation of  $\mathbf{u}_v$  by the angles  $\alpha_i$  and  $\beta_i$ , the transformation of input coordinates can be described as follow:

- 1) For a fixed propeller,  $u_{l,i}$  corresponds to  $u_{\lambda,i}$ .
- 2) For a propeller with only radial tilting,  $\mathbf{u}_{l,i} = [u_{\lambda,i} \cos(\alpha_i) \quad u_{\lambda,i} \sin(\alpha_i)]^\top$ .
- 3) For a propeller with only tangential tilting,  $\mathbf{u}_{l,i} = [u_{\lambda,i} \cos(\beta_i) \quad u_{\lambda,i} \sin(\beta_i)]^\top$ .
- 4) For a propeller tilting in  $\mathbb{S}^2$

$$\mathbf{u}_{l,i} = \begin{bmatrix} u_{\lambda,i} \sin(\alpha_i) \\ u_{\lambda,i} \cos(\alpha_i) \cos(\beta_i) \\ u_{\lambda,i} \cos(\alpha_i) \sin(\beta_i) \end{bmatrix} \quad (20)$$

We represent  $\mathfrak{F}_1$  as the discrete set of forces  $\mathbf{f}_d$ , for which the computed  $\mathbf{u}_d = \mathbf{F}_l^\dagger [\mathbf{f}_d^\top, \mathbf{0}_3^\top]^\top \in \mathbb{U}$ .

*c) Case 3: Jointly tilted propellers:* We represent  $\mathfrak{F}_1$  as the discrete set of forces  $\mathbf{f}_d$ , for which the numerical optimization  $\|\mathbf{F}(\alpha, \beta) \mathbf{u}_\lambda - [\mathbf{f}_d^\top, \mathbf{0}_3^\top]^\top\|_2^2$ , with the constraint  $\mathbf{u} \in \mathbb{U}$  reaches a valid solution. To find such a solution, we employ a gradient-based method such as the one presented in (Byrd et al. 2000).

## F. System Abilities

The system abilities are expressed w.r.t. the tasks that can be achieved by the multirotor based on its design, and are all directly related to the possible wrench space  $\mathbb{W}$ . We divided these tasks in three representative categories that encompass the variety of tasks that can be achieved by multirotor systems.

In what follows we detail the platform abilities:

1) *Hovering Ability*: The ability to hover corresponds to the ability of the platform to stay stationary at the desired position. This represents the main advantage of multirotors over fixed wings UAVs.

In details, in the scope of this manuscript, we define the *static hovering* as the ability of the platform to stabilize its position and orientation for some orientation  ${}^W\mathbf{R}_B \in \text{SO}(3)$  with zero linear and angular velocity (i.e.,  $({}^W\mathbf{p}_B, {}^W\mathbf{R}_B, {}^B\dot{\mathbf{p}}_B, {}^B\boldsymbol{\omega}_B) = ({}^W\mathbf{p}_B, {}^W\mathbf{R}_B, \mathbf{0}, \mathbf{0})$ ). This can be achieved (as described in (Micheletto et al. 2018)) if at  ${}^W\mathbf{R}_B$

$$\exists \mathbf{u}^* \in \mathbb{U} \text{ s.t. } \begin{cases} \mathbf{f}(\mathbf{u}^*) = m\mathbf{g}e_3 \\ \mathbf{m}(\mathbf{u}^*) = \mathbf{0}_3 \\ \text{rank}\{\mathbf{F}\} \geq 4 \end{cases} . \quad (21)$$

Finally, we define *dynamic hovering* (or relaxed hovering) as the ability of the platform to roughly stabilize its position while varying its linear and angular velocity. In other words, for these platforms static hovering is not feasible, i.e.,  $\nexists \mathbf{u}^* \in \mathbb{U}$  s.t. for  ${}^W\mathbf{R}_B$ ,  $({}^B\dot{\mathbf{p}}_B, {}^B\boldsymbol{\omega}_B) = (\mathbf{0}, \mathbf{0})$ , however, hovering is achieved through continuous control of the platform.

Following the above definitions, we define the following categories of hovering:

- H.0** hovering not possible (e.g., fixed-wing UAVs)
- H.1** dynamic hovering (relaxed hovering)
- H.2** hovering in a single orientation (e.g., quadrotor)
- H.3** hovering in several orientations (e.g., the TiltHex design shown in (Ryll, Muscio, et al. 2017))
- H.4** hovering in any orientation (e.g., omnidirectional UAVs).

Categories **H.2**, **H.3**, and **H.4** are subclasses of the family of platforms that can achieve static hovering, with the possible orientations spanning an increasingly large space. We remark that each ability from **H.1** to **H.4** includes the previous abilities.

2) *Trajectory Tracking Ability*: The ability to follow a trajectory is fundamental for many multirotor applications such as survey, surveillance, and delivery. We propose to categorize the trajectory tracking ability based on the type (position and orientation) and the number of degrees of freedoms (DoFs) the multirotor can track independently. While some platforms can trade off the tracking in position for its orientation counterpart, in our classification we consider positional tracking to have a higher priority than orientation tracking. As such we consider the 3D position tracking ability as a baseline for the tracking ability classifications listed below:

- TT.1** 3D position
- TT.2** 3D position + 1D orientation (e.g., quadrotors)
- TT.3** 3D position + 2D orientation
- TT.4** 3D position + 3D orientation

3) *Physical Interaction Ability*: We also consider the ability to physically interact with the environment, following the rising trend of *aerial physical interaction* (APhI) in the last decade. In particular, we decided to separate the possible APhI abilities according to the following classifications:

- APhI.0** APhI not possible
- APhI.1** suitable for tasks like pushing/pulling
- APhI.2** suitable for tethered APhI
- APhI.3** suitable for carrying a load
- APhI.4** suitable for manipulation tasks

It should be noted that the APhI abilities require suitable hardware for the specific task, and an adequate level of force and moment decoupling. As explained in (Micheletto et al. 2018), the decoupling between force and moment allows a platform to apply forces in one or more directions while applying null moment. This is a requirement to physically interact with a static environment while maintaining hoverability. It should be noted that the force-moment decoupling of a design can be derived from the study of its full allocation matrix  $\mathbf{F}$  (Micheletto et al. 2018).

As the APhI ability depends not only on the platform property (e.g., full allocation matrix) but also on the externally attached hardware, for each platform, we characterize two APhI properties: i) the true APhI ability as demonstrated by the authors of the platform; ii) the theoretical APhI ability that can be reached if an adequate tool (like a manipulator) was added to the platform.

4) *Level of Maturity*: Given the vast literature on multirotor design, we decided to also stress the level of maturity to distinguish purely theoretical contributions from designs that have been constructed and tested in various scenarios. While the theoretical grounding of any design is of paramount importance, we believe that each should be tested by real experiments verifying the corresponding findings. To this goal, we include in our assessment the level of maturity of each design, where the level can be one of the following:

- 1) theory,
- 2) simulation of the simplified model (simplistic simulation),
- 3) simulation with uncertainties and/or second order effects (realistic simulation)
- 4) prototype, and
- 5) product.

Results dimmed as theoretical comprise work where the analysis of the design is conducted without any simulation or prototype. On the other hand, we separate simulation proven designs into two categories, where simplistic simulations that serve as a proof of concept are distinguished from realistic ones, which include delays, noise, model discrepancies, external perturbations and so on. The latter reflects a higher degree of maturity of the work and a smaller gap to real experiments. Finally, we label as prototype any work presenting a functional prototype of the proposed design. The final level of maturity would describe designs implemented as commercial products, but we note that such occurrences are rare.

## III. UNIROTOR (1 AAU)

Even though the case of a multi-rotor composed of a single AAU is a contradiction in itself, it is considered for complete-

apparition	properties	abilities	maturity
Zhang et al. 2016	none	H.1, TT.1, APhI.0	prototype

TABLE V: Recapitulative table for  $N = 1$ .

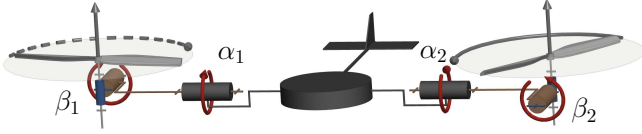


Fig. 2: Conceptual 3D kinematic representation of a generic birotor design with wing-tail stabilization.

ness of the review; in addition, it can represent a configuration reached in the case of extreme failure of multi-rotors. To the best of the authors' knowledge, the only occurrence of such design, fitting this paper scope, *i.e.*, exclusion of moving mass and control surface, can be found in (Zhang et al. 2016).

The proposed approach relies on active control and demonstrates a position tracking controller for such a vehicle. Due to its single rotor  $n_u = 1$ , the vehicle is under constant rotation, however, the prototype was shown to be able to achieve relaxed hovering. The system assessment is shown in Table V.

#### IV. BIROTOR (2 AAUS)

Birotors are composed of only two AAUs as their name suggests. For these designs, hovering can only be achieved if thrust vectoring is controlled, *i.e.*, the total thrust is dynamically oriented during flight. The two AAUs are always rotating in opposing directions to have a zero total drag moment when the propellers spin at the same speed, thus the platform can hover without being subjected to constant rotation. In addition, in most designs, the multirotor CoM is placed between the two AAUs to benefit from a damped pendulum dynamics, such as the work in (Chowdhury et al. 2012), where a wing-tail was also added for stabilization as shown in Fig. 2.

##### A. Tilting in $S^2$ Designs

The first pioneer work on bi-rotor design was (Gress 2002), in which the inertia and gyroscopic characteristics of the multirotor are exploited to control the roll, pitch, and yaw in order to achieve a stable hover. The two AAUs are devised to be tilting in  $S^2$  independently, thus  $n_u = 2 + 4$  as shown in Fig. 2. Further studies were conducted by Kendoul et al. 2006 and Amiri et al. 2011, providing the dynamic model of such designs and introducing some refinements to increase controllability. In the latter, the two AAUs generate unidirectional thrust actuated independently in  $S^2$ . As the resulting dynamic model is highly non-linear and hard to exploit for control purposes, a simplified model is introduced in (Kendoul et al. 2006) which allows considering backstepping approaches for control.

Another platform presenting propellers tilting in  $S^2$  was proposed in (Sanchez et al. 2008), where the authors consider the same design as in (Gress 2002) (Fig. 2) while enforcing both AAUs to have the same tilting angles, leading to

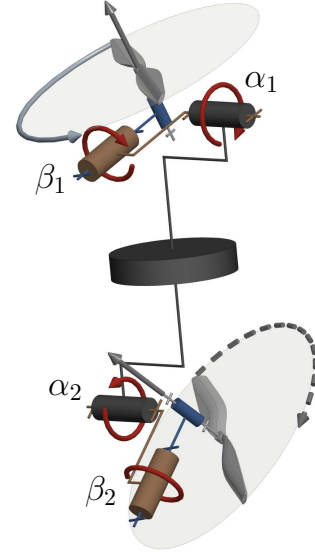


Fig. 3: Conceptual 3D kinematic representation of the birotor design presented in (Prothin and Moschetta 2013).

$n_u = 2 + 2$ . This design reduces the computational complexity of the control while still being able to achieve hovering in the conducted experiments.

In Prothin and Moschetta 2013 the authors present another design, named the 'donut', made of two AAUs aligned vertically with the center of the multirotor frame, which can be tilted independently in  $S^2$  as shown in Fig. 3, thus obtaining again  $n_u = 2 + 4$ . The details of the dynamical model are presented and the authors propose to leverage the tilting to use drift force and moment as control inputs.

##### B. Radial and Tangential Tilting Designs

A birotor design often found in the literature is presented in Papachristos et al. 2011, where the platform has two AAUs placed on an axis above the CoM of the platform, and tilting independently radially about their axis, thus resulting in  $n_u = 2 + 2$ . This design provides the option to tilt almost perpendicularly to the vertical direction, and thus the platform can generate most of its lift laterally to redirect its lift in the desired flight direction. In this design, yaw is achieved by tilting propellers about opposite  $\alpha$  angles, roll is achieved by applying different thrust in each propeller, and pitch is achieved by tilting both propellers equally in the direction of the desired pitch, where the pitching moment is relative to the tilting angle and the vertical distance between the propellers CoM and the platform CoM. This design is illustrated in Fig. 2.

A similar design was shown in (Chowdhury et al. 2012), where the authors propose a controller that changes the tilt angles to achieve desired roll and yaw independently and demonstrate their controller in simulation. Another such controller was proposed in (Blouin and Lantaigne 2014), however, they test their controller on a prototype. Finally, Cardoso et al. 2016 present a robust controller for this platform design and showed its path tracking ability in a realistic simulation under external disturbances and model uncertainties.

apparition	$n_u$	DoF	properties	abilities	maturity	figure
Gress 2002 Kendoul et al. 2006 Amiri et al. 2011	2+4	$\alpha_1, \alpha_2, \beta_1, \beta_2$	MDT	H.3, TT.2, APhI.0/APhI.4	prototype	Fig. 2
Sanchez et al. 2008	2+2	$(\alpha_1, \alpha_2) (\beta_1, \beta_2)$	UDT	H.2, TT.2, APhI.0/APhI.3	prototype	Fig. 2
Donadel et al. 2014	2+2	$\beta_1, \beta_2$	UDT	H.2, TT.2, APhI.0/APhI.3	realistic simulation	Fig. 2
Prothin and Moschetta 2013	2+4	$\alpha_1, \alpha_2, \beta_1, \beta_2$	MDT	H.3, TT.2, APhI.0/APhI.4	prototype	Fig. 3
Papachristos et al. 2011	2+2	$\alpha_1, \alpha_2$	UDT	H.2, TT.2, APhI.0/APhI.3	prototype	Fig. 2
Chowdhury et al. 2012	2+2	$\alpha_1, \alpha_2$	UDT	H.2, TT.2, APhI.0/APhI.3	simplistic simulation	Fig. 2
Blouin and Lanteigne 2014	2+2	$\alpha_1, \alpha_2$	UDT	H.2, TT.2, APhI.0/APhI.3	prototype	Fig. 2
Cardoso et al. 2016	2+2	$\alpha_1, \alpha_2$	UDT	H.2, TT.2, APhI.0/APhI.3	realistic simulation	Fig. 2

TABLE VI: Recapitulative table for the birotors ( $N = 2$ ).

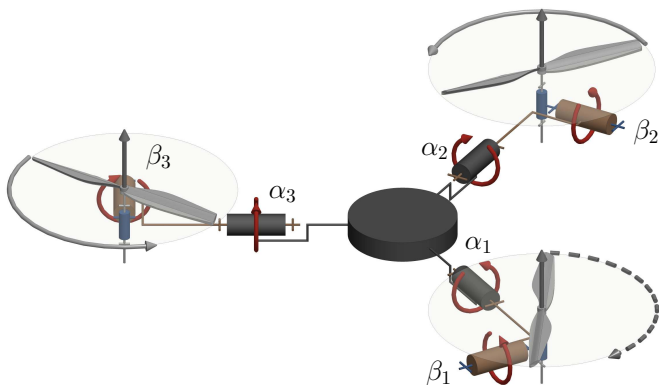


Fig. 4: Conceptual 3D kinematic representation of a generic trirotor  $\Delta$ -configuration design.

In (Donadel et al. 2014) the authors propose a design where the tangential tiltings are fixed and the two radial tiltings are actuated, hence, again,  $n_u = 2 + 2$ , with propellers CoM also above the CoM of the platform as shown in Fig. 2. They propose a control approach relying on optimal  $H_\infty/H_2$  techniques, which they validated in realistic simulations.

### V. TRIROTOR (3 AAUS)

Trirotors are composed of three AAUs. As such, can be considered as an upgrade from birotors, but they pose a challenge due to the unbalanced moment caused by the odd number of propellers. In addition, and similarly to birotors, the few numbers of actuators imposes limitations on the achievable performance, in particular in the ability to perform stable hovering (Kataoka et al. 2011).

One of the first trirotor designs appeared in (Rongier et al. 2005), where propellers are tilted at a fixed angle so that a non-collinear thrust is ensured. The control is based on a combination of aircraft gyroscopic effect with a piezosensor to detect the tilt angle (pitch and roll) with respect to the horizontal orientation. However, the lack of control of the yaw angle forces the rotor to constantly rotate about its CoM, thus being unable to achieve the basic static hovering ability (H.2). The design is demonstrated on a prototype powered with a cable and shown in Fig. 4; as the platform constantly rotates, it stretches the cable causing a failure of the proposed controller.

Multiple designs have been later proposed in the literature that aim to balance the odd shape of the trirotor, which we

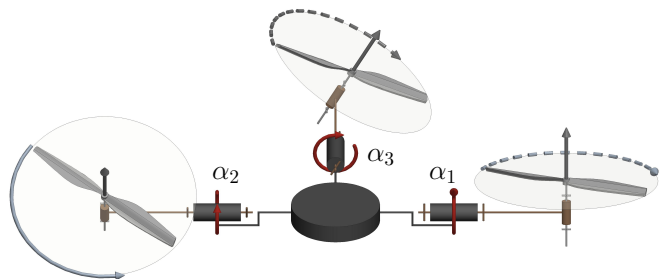


Fig. 5: Conceptual 3D kinematic representation of a generic trirotor T-configuration design. The tail propeller (typically smaller and weaker) is depicted on the top while the frontal principal propellers (typically larger and stronger) are on the bottom. The sagittal axis points down in the picture.

group into *T-configurations* and  *$\Delta$ -configurations*. In addition, to overcome the limitation of the number of actuators, which are not enough to achieve the basic H.2, several works have proposed to add one or more additional actuators in order to achieve thrust-vectoring, thus making the platform able to gain the H.2 ability.

#### A. T-Configuration

This setup is composed by two frontal *principal propellers*, that may be dynamically tilted or fixed, spinning in opposite directions, with a third propeller (typically smaller) mounted on a *tail* as shown in Fig. 5. This one, in general, tilts around the radial axis in order to improve pitch and yaw control.

1) *Tail-only tilting propeller*: this design was presented in (Salazar-Cruz and Lozano 2005), followed by (Salazar-Cruz, Lozano, and Escareño 2009). The *tail-propeller* is endowed with a servo motor which allows the control of the yaw motion by tilting about the sagittal axis, and the pitch angle regulating the propeller rotational speed. The two main frontal fixed propellers are in charge of the control of total thrust and roll angle. In total we have  $n_u = 3 + 1$ . The  $\mathfrak{F}_1$  space is represented in Fig. 6.

In the mentioned works, the hovering and the forward flight control of this vehicle were achieved using a nonlinear controller based on nested saturations. The same design is instead controlled in (Yoon et al. 2013) with an optimal LQR to control the attitude. All these works have been validated with an experimental prototype.

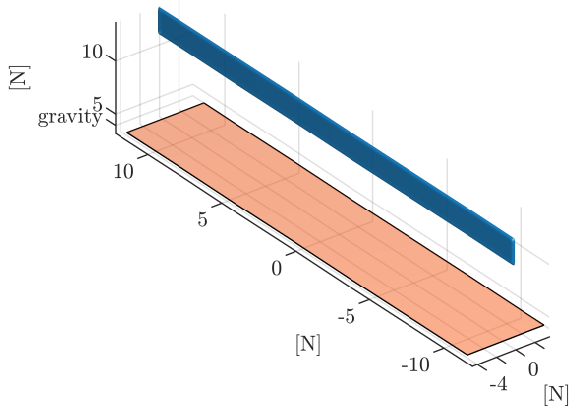


Fig. 6: visualization of the  $\mathfrak{F}_1$  space of the design presented in (Salazar-Cruz, Lozano, and Escareño 2009) in blue, and the corresponding gravity plane in orange. T-shaped trirotor with tail tilting radially and with two fixed main propellers.  $N = 3$  and  $n_u = 3 + 1$ . Profile description: 2D plane perpendicular to the tail rotation plane.

2) *Frontal-propeller tilting*: In a design presented in (Papachristos and Tzes 2013), (Papachristos et al. 2014) and (Papachristos et al. 2016), the two frontal principal propellers are also able to tilt radially with the same (locked) tilting angle, while the tail rotor can tilt independently, thus obtaining  $n_u = 3 + 2$ . This approach was adopted to allow the vehicle to apply a push-force (A<sub>PhI.1</sub>) in the sagittal direction. To improve the control scheme and platform stability, in (Papachristos et al. 2016) an MPC (Model Predictive Control) approach was implemented.

A commercially available T-configuration trirotor is the *Cerberus Tilt-Rotor*<sup>4</sup>. In this product the two frontal principal propellers can tilt radially independently, while the tail propeller is fixed, thus obtaining again  $n_u = 3 + 2$ . However, its kinematics is different than the previous one. The  $\mathfrak{F}_1$  space of the Cerberus Tilt-Rotor is similar to the  $\mathfrak{F}_1$  space represented in Fig. 6.

### B. $\Delta$ -Configuration

This design is composed of three propellers of the same dimension arranged on a triangle, with two of them spinning in opposite directions. In addition, in these configurations the thrust is roughly shared equally by all three motors, encouraging the symmetrical placement of the motors on a circle (*i.e.*, every  $2\pi/3$ ) as shown in Fig. 4.

One example design was presented in (Escareno et al. 2008), where the authors built a  $\Delta$ -configuration multirotor with all propellers being allowed to tilt radially with the same angle, thus obtaining  $n_u = 3 + 1$ . While the propellers' tilting is used to directly control the yaw motion, its effect on pitch and roll behavior is compensated as a disturbance. The overall control system is robust with respect to dynamic couplings, in particular gyroscopic effects, and shows a maneuverability similar to that of a quadrotor but with a more compact design

<sup>4</sup><http://skybornotech.com/>

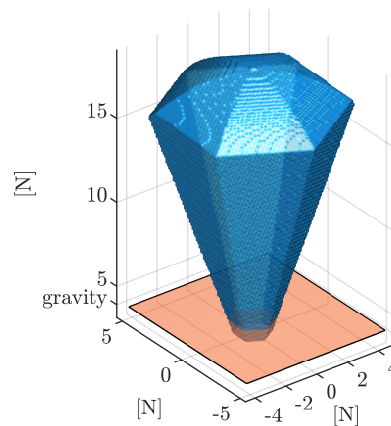


Fig. 7: visualization of the  $\mathfrak{F}_1$  space of a  $\Delta$ -trirotor with independent radial tilting of all three propellers; tilting angle limits are chosen at  $\pm 30^\circ$ . The corresponding gravity plane is shown in orange.  $N = 3$  and  $n_u = 6$ . Profile description: hexagonal pyramid with the tip at zero enclosed with a dome.

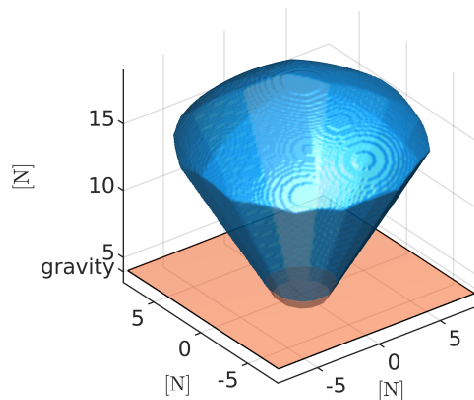


Fig. 8: visualization of the  $\mathfrak{F}_1$  space of the design presented in (Ramp and Papadopoulos 2015). The design consists of a  $\Delta$ -trirotor with all propellers independently tilting both radially and tangentially; tilting angle limits are chosen at  $\pm 30^\circ$ . The corresponding gravity plane is shown in orange.  $N = 3$  and  $n_u = 9$ . Profile description: dodecagonal pyramid with the tip at zero with top enclosed with a dome.

as well as a longer autonomy, thanks to the fewer number of motors.

Another  $\Delta$ -configuration design was presented in Mohamed and Lanson 2012, where each propeller can be titled independently in its radial direction in a range of  $[-\pi/2, \pi/2]$ , thus obtaining  $n_u = 3 + 3$ . The resulting is a fully actuated vehicle, controlled with  $H_\infty$  loop shaping, and achieving full-pose tracking. Similar designs were studied in (Kastelan et al. 2015), (Servais, Mounier, et al. 2015), and (Servais, d'Andréa-Novel, et al. 2015), and the  $\mathfrak{F}_1$  space of such designs is represented in Fig. 7.

On the other hand, Ramp and Papadopoulos 2015 present an overactuated system, where each of the three propellers is allowed to rotate independently in both its tangential and radial direction, thus obtaining  $n_u = 3 + 6$ . This overactuated system was tested in a realistic simulation, where it proved its ability to achieve full-pose tracking, and we provide its  $\mathfrak{F}_1$

apparition	$n_u$	DoF	properties	abilities	maturity	figure
Rongier et al. 2005	3			H.1, TT.1, APhI.0	prototype	Fig. 4
Salazar-Cruz and Lozano 2005	3+1	$\alpha_3$	UDT	H.2, TT.2, APhI.0/APhI.3	prototype	Fig. 5
Salazar-Cruz, Lozano, and Escareño 2009						
Yoon et al. 2013						
Papachristos and Tzes 2013	3+2	$(\alpha_1, \alpha_2), \alpha_3$	MDT	H.2, TT.2, APhI.1/APhI.3	prototype	Fig. 5
Papachristos et al. 2014						
Papachristos et al. 2016						
<i>Cerberus RC Tilt-Rotor</i>	3+2	$\alpha_1, \alpha_2$	MDT	H.3, TT.3, APhI.0/APhI.3	product	Fig. 5
Escareno et al. 2008	3+1	$(\alpha_1, \alpha_2, \alpha_3)$	UDT	H.2, TT.2, APhI.0/APhI.3	prototype	Fig. 4
Mohamed and Lanzon 2012	3+3	$\alpha_1, \alpha_2, \alpha_3$	FA	H.3, TT.4, APhI.0/APhI.4	simplistic simulation	Fig. 4
Kastelan et al. 2015	3+3	$\alpha_1, \alpha_2, \alpha_3$	FA	H.3, TT.4, APhI.0/APhI.4	prototype	Fig. 4
Servais, Mounier, et al. 2015	3+3	$\alpha_1, \alpha_2, \alpha_3$	FA	H.3, TT.4, APhI.0/APhI.4	prototype	Fig. 4
Servais, d'Andréa-Novel, et al. 2015						
Ramp and Papadopoulos 2015	3+6	$\alpha_1, \alpha_2, \alpha_3, \beta_1, \beta_2, \beta_3$	OA	H.3, TT.4, APhI.0/APhI.4	realistic simulation	Fig. 4

TABLE VII: Recapulative table for the trirotors ( $N = 3$ ).

space in Fig. 8. To find the desired thrust and orientations, the controller is designed to find the desired force vector for each propeller independently, which is then achieved by reorienting the propeller to the desired direction and applying the desired thrust.

Table VII summarizes all the presented designs.

## VI. QUADROTOR (4 AAUs)

This case is of particular interest because for designs with fixed AAUs,  $N = 4$  is the minimum number of propellers necessary to achieve the basic actuation assumptions summarized in (10) and (11), in addition to the UDT property and the static hoverability ability **H.2**.

The first documented quadrotor design in the literature traces back to 1907 and documented in (Young 1982). While this design recorded a few tethered flights, the modern quadrotor design (Pounds, Robert Mahony, Hynes, et al. 2002) traces its origin back to the same platform concept, however, technological advancements within the last century has allowed new platforms to be built with compact electronics and sensors, allowing robust and agile maneuvers.

While the first designs relied on a coplanar/collinear propeller configuration, later modifications were conducted to extend the system properties via thrust-vectoring. All the presented designs consider the AAUs and the CoM to be located roughly on the same plane. We refer to Table. VIII as a summary of the presented designs.

### A. Coplanar/collinear Designs

For modeling, control and the general theory of classical coplanar/collinear designs one can refer to (R. Mahony et al. 2012; Bouabdallah, Noth, et al. 2004; Bouabdallah and Siegwart 2005; Pounds, Robert Mahony, and Corke 2010), which are three comprehensive references among the vast literature of such designs. We present an example of  $\mathfrak{F}_1$  space of such designs in Fig. 9. Note that the designs with less than 4 AAUs cannot obtain such nice mono-dimensional shape (UDT ability) because they need at least a tilting rotor to achieve the static hovering (H.2). This makes the coplanar/collinear quadrotor the simplest platform of its kind, i.e., with a minimum number of total inputs (servo- and brushless motors) that

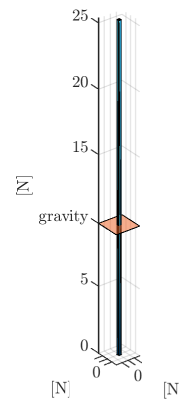


Fig. 9: visualization of the  $\mathfrak{F}_1$  space of a fixed coplanar/collinear quadrotor design. The corresponding gravity plane is shown in orange.  $N = 4$  and  $n_u = 4$ . Profile description: line along the CoM of the platform.

has a decoupled force and moment spaces. Such decoupling simplifies significantly the control problem and is one of the reasons for the success of quadrotors.

Note that the wide attention gathered by coplanar/collinear quadrotors comes from the combination they offer between their simple mechanics and relative easiness of control for trajectory tracking, thanks to the dynamic feedback linearizability (or, equivalently, the differential flatness) of the nonlinear system (Mistler et al. 2001).

This enabled a vast set of applications for coplanar/collinear designs. Innovative modular designs such as the one presented in (Zhao et al. 2017), exhibit the same properties as classical coplanar/collinear designs, although they lie outside the scope of this paper due to their varying CoM with each new configuration.

Additionally, coplanar/collinear designs for  $N > 4$ , shown in Fig. 10, (typically  $N = 6$  or  $N = 8$ ) will not be discussed hereafter as their properties are the same as the  $N = 4$  case. Their coplanar/collinear distribution leads to similar results for all such designs despite the increase of the control inputs. The only notable differences are 1) the increase of the control authority due to the increase of AAUs, which translates mostly

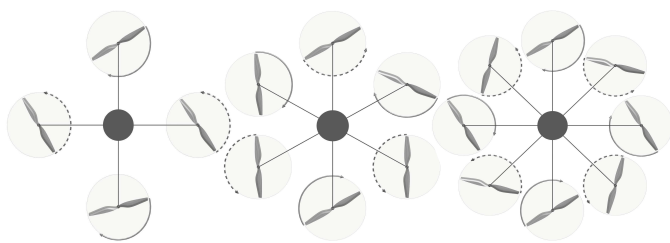


Fig. 10: Top view of the conceptual kinematic representation of coplanar designs with (left to right) 4/6/8 propellers.

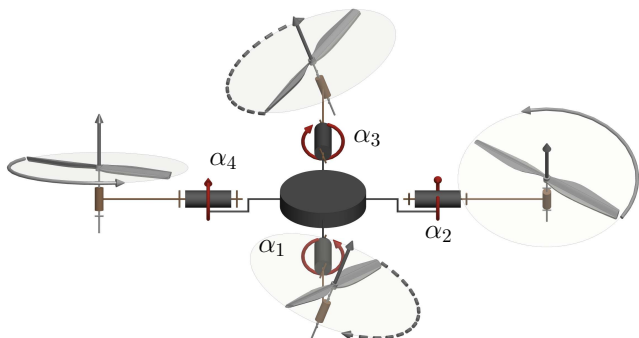


Fig. 11: Conceptual 3D kinematic representation of a generic quadrotor with propellers tilting/tilted about their radial axes.

in an increase of payload, and 2) the possible redundancy, *i.e.*, AAUs failure can be mitigated while preserving the quadrotor properties.

### B. Radial Tilting Designs

Some designs consider AAUs which are radially tilted/tilting in order to achieve total thrust vectoring for quadrotors as shown in Fig. 11. Within the other two

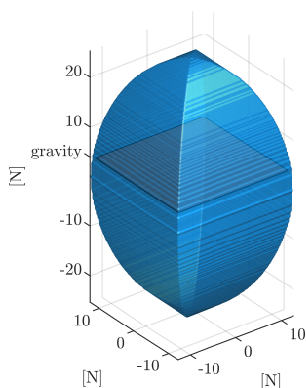


Fig. 12: visualization of the  $\mathfrak{F}_1$  space of the design presented in (Ryll et al. 2012). The design consists of a quadrotor with all propellers independently tilting about their corresponding radial axis. The corresponding gravity plane is shown in orange.  $N = 4$  and  $n_u = 8$ .

tilting directions, this particular design can be considered as the simplest mechanical extension to the coplanar/collinear design achieving thrust vectoring.

Falanga et al. 2017 present a quadrotor with propellers tilted  $15^\circ$  radially about their relative axes, *i.e.*,  $n_u = 4$ . The tilt angle is computed to increase yaw-control, and was tested on a prototype flying through a narrow gap. The design is shown in Fig. 11.

Ryll et al. 2012 proposed a configuration, further analyzed in (Ryll et al. 2013) and (Ryll et al. 2015), where four additional servomotors are used to independently radially tilt the AAUs, thus obtaining  $n_u = 4 + 4$ , resulting in an over-actuated system, with  $\mathfrak{F}_1$  space presented in Fig. 12. By considering the servo dynamics and the aerodynamic effects, the authors derive and propose a highly coupled system, which proves difficult to manage from a control point of view. To mitigate these shortcomings, the classical approach neglects the servo-motor dynamics and assumes the employment of high gain controllers which can achieve instantaneous tracking. In addition, the aerodynamic effects are modeled in the controller as external disturbances. These simplifications allow the use of feedback linearization techniques with dynamic extension, for a desired trajectory tracking of class  $\mathcal{C}^3$ . The system overactuation is dealt with a pseudo-inverse allocation, that is used to obtain a minimum energy thrust generation. The design and corresponding controller have been validated through simulation and experimental implementation.

In (Falconi and Melchiorri 2012) a similar design was considered with the implementation of an inverse dynamic controller, to compensate for the nonlinear dynamics, and a PD with feedforward to impose a position and attitude trajectory. Similarly to Ryll et al. 2015, Falconi and Melchiorri 2012 solved the allocation problem using a pseudo-inverse approach. This approach is more sensitive to model uncertainty due to the complexity of the aerodynamic modeling.

In (Oosedo et al. 2016), the authors study a wide range of platform orientations in addition to the transition from horizontal to vertical hovering of the multirotor. Position and orientation are regulated through a PID loop while control allocation techniques for two orientation sets are proposed and experimentally validated.

In (Yih 2016) the authors considered the same design subjected to model uncertainties. They propose a robust sliding mode controller for position and orientation tracking, augmented with a chattering suppression block to improve its performance. The proposed model and control law were validated in simulation.

In (Nemati and Kumar 2014) similar radial tilting of the AAUs is considered while constraining paired AAUs to tilt the same angle in opposing directions, thus obtaining  $n_u = 4 + 2$ . This results in a fully actuated system (non-overactuated). A trajectory tracking goal has been achieved by PD regulators. In (Nemati, Soni, et al. 2016) the described design is built and tested.

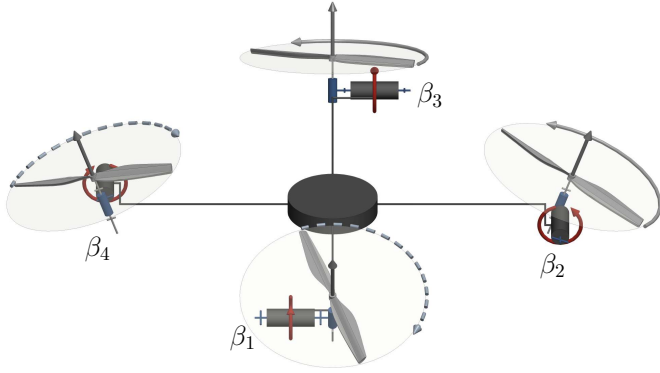


Fig. 13: Conceptual 3D kinematic representation of a generic quadrotor with propellers tilting/tilted about their tangential axes.

### C. Tangential Tilting Designs

Another attempt at extending the classical quadrotor design is to consider tangential tilting of the AAUs, see Fig. 13, as in (Badr et al. 2016), which has also  $n_u = 8$ . To maintain the moment balanced, the AAUs rotation direction is non-standard. Indeed usually CW and CCW AAUs are alternating along the four summits of their square distribution, but in this proposed design they are grouped two by two. This choice allows to have more control authority for pitch and roll motions while decoupling roll from the y-translation and pitch from the x-translation. In (Badr et al. 2016), the authors develop a controller that resorts to simplifying assumptions based on the trajectory characteristics. This control is tested for a simple trajectory in simulation to validate the decoupling between rotational and translational dynamics. A similar design to the latter was presented by Devlin et al. 2018, with each propeller rotating independently in the tangential direction, thus obtaining again  $n_u = 4 + 4$ . The platform is named *ElbowQuad*. The design was tested via a real experiment on a prototype of the design.

In (Scholz et al. 2016), the authors also study the design shown in Fig. 13. To control the platform they synchronized the rotational speed of each of the four AAUs, then derive an input allocation scheme based on heuristics and propose a backstepping approach. The controller tracks the desired orientation, altitude and velocity in the plane, and is robust to unmodeled dynamics. The authors rely on optimization techniques to tune the controller gains. This approach is corroborated with simulation comprising sensor noise.

Another design with tangential tilting of the AAUs can be found in (Long, Lyttle, et al. 2012), with  $n_u = 4 + 4$ , and (Long, Gelardos, et al. 2014), with  $n_u = 4 + 3$ , named *Omnicopter*. The latter is shown in Fig. 14. In this proposed design one main AAU (with either one or two propellers sharing the same axis of rotation with opposed rotation directions) is significantly bigger than the other propellers and is placed in the center of the platform with its thrust direction aligned with the  $\mathbf{z}_B$  axis of the body frame. The other three AAUs, smaller in size, are distributed around the main one in a triangular distribution and allowed to tilt tangentially.

In (Long, Lyttle, et al. 2012) a backstepping approach and

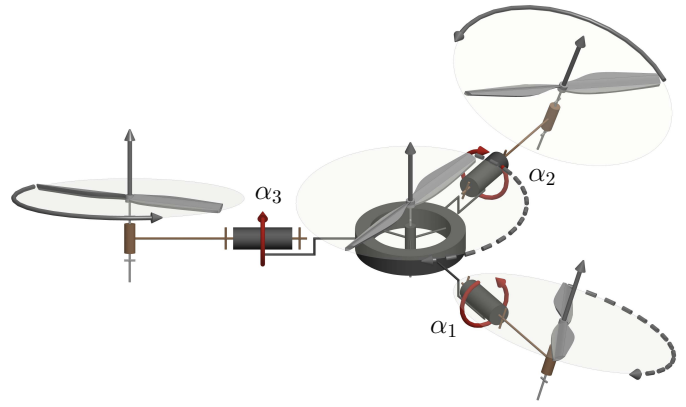


Fig. 14: Conceptual 3D kinematic representation of the quadrotor design presented in (Long, Lyttle, et al. 2012; Long, Gelardos, et al. 2014). The three non-central propellers are tilting about their radial axes independently.

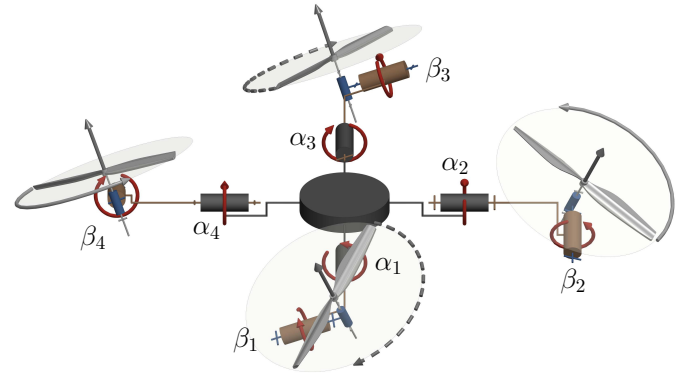


Fig. 15: Conceptual 3D kinematic representation of a generic quadrotor with propellers tilting/tilted in  $\mathbb{S}^2$ , i.e., about both the radial and tangential axes.

PID loop are used to achieve decoupled tracking of both orientation and position. The control allocation is achieved by considering a linearization of the system around the functioning point. In (Long, Gelardos, et al. 2014) the authors proposed the same design with only one central AAU to improve the efficiency of the design. They apply the same control technique for the second design and validate both designs via real experimentations on a prototype.

### D. Tilting in $\mathbb{S}^2$ Designs

The following designs explore the AAUs tilting in  $\mathbb{S}^2$  as illustrated in Fig. 15, in order to achieve thrust vectoring in all directions for each AAU. Note that due to the mechanical complexity involved in such a design, most of the presented work considering non-fixed AAUs are only theoretical studied.

The first original design can be found in (Şenkul and Altuğ 2013) and (Şenkul and Altuğ 2014), where the authors consider a classical quadrotor with each AAU being able to tilt both radially and tangentially. In the first work the authors consider all AAUs to tilt independently while rotating at the same speed, hence  $n_u = 1 + 8$ . Then the full potential of this design is exploited in (Şenkul and Altuğ 2014), where the authors allow independent tilting of the propellers,  $n_u = 4 + 8$ .

The authors propose a cascaded PID control loop with adaptive gains to account for the gyroscopic effect arising from the propellers. The above two approaches are validated with simple simulations to show their trajectory tracking ability.

Similarly to Şenkul and Altuğ 2013, Hua et al. 2015 propose to study a quadrotor tilting in  $S^2$  as shown in Fig. 16 such that the total thrust vectoring is achieved by tilting each AAU equally in the same thrust direction. This scheme allows the platform to apply uni-directional thrust but in a direction that is tiltable in  $S^2$  thus obtaining  $n_u = 4+2$ . The authors propose a control scheme that primarily tracks a reference position or velocity (similar to a coplanar/collinear quadrotor with fixed propellers), then rotates the thrust direction to point in the desired orientation. Position and orientation are proved to be decoupled, which is validated in a simple trajectory tracking simulation.

The same design shown in Fig. 16 is explored in (Odelga et al. 2016), with the addition of an explicit mechanism design that enforces the angles to rotate equally, while in (Hua et al. 2015) it was only theoretically assumed. Full-actuation allows using a standard feedback linearization control with dynamic extension, which is validated by simulation. The introduction of a real mechanism makes explicit the constraints induced by the mechanism limits. Therefore, tracking performances are limited by unidirectional rotors and tilt angle limits, despite the full actuation nature of the design.

De Martini et al. 2017 also present a quadrotor design with propellers tilting synchronously in  $S^2$  as shown in Fig. 15. The synchronization allows the vehicle to fly across a narrow passage, where each pair of propellers are assumed to be tilting about a given axis, with  $n_u = 4 + 2$ . Furthermore, bidirectional AAUs are considered and physical mechanism constraints are neglected. The proposed control scheme is based on PID and model inversion and validated in a simple simulation. The multirotor orientation is computed in order to allow the navigation through the narrow passage geometry.

The above contributions presented analysis and simulations studying quadrotors with propellers tilting in  $S^2$ . In what follows we introduce the contributions that presented a working mechanical system with propellers either tilting in  $S^2$ , or tilted about a fixed orientation throughout their flight.

In (Khoo et al. 2017), the authors implement a design as shown in Fig. 15 that allows independent rotation of all propellers, thus obtaining  $n_u = 4 + 8$ . The prototype is controlled with a multi-surface sliding mode controller, followed by a pseudo-inverse control allocation.

In (Segui-Gasco et al. 2014) the authors also build a prototype, while considering tilting limits of each AAU in its control. The dynamics of the system are derived while considering the gyroscopic moment produced by the fast tilting AAUs. The authors consider a coplanar/collinear quadrotor controller, with body orientation and total thrust calculated through system linearization and weighted pseudo-inverse. The over-actuation of the system calls for control allocation, which is calculated in an energy-optimal way. The authors validated their approach with a hovering maiden flight, and their design analysis suggested the need for high inertia propellers to increase the produced torque and allow higher vehicle speeds.

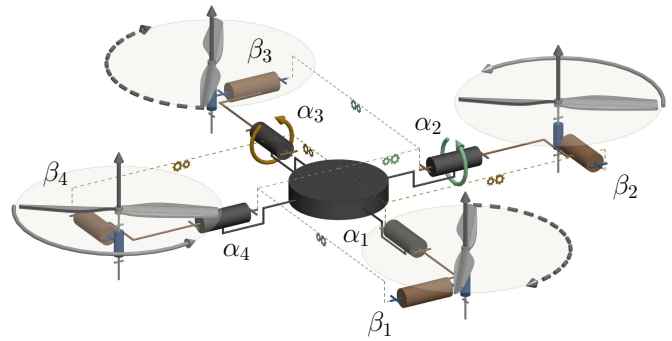


Fig. 16: Conceptual 3D kinematic representation of a quadrotor with propellers tilting/tilted in  $S^2$  presented in (Hua et al. 2015; Odelga et al. 2016). Highlighted the locked tilting that makes all the propellers point always in the same direction.

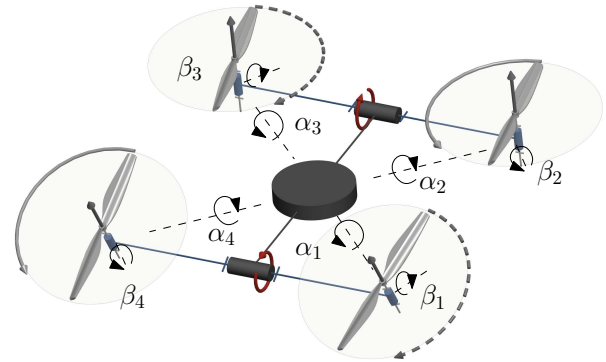


Fig. 17: Conceptual 3D kinematic representation of a quadrotor with propellers tilting  $s$  in  $S^2$  as presented in (Kawasaki et al. 2015).

Another design with the AAUs tilting in  $S^2$  can be found in (Kawasaki et al. 2015), where the authors propose a design such that the AAUs are tilted independently by pairs as shown in Fig. 17, where we can see that each pair of propellers are connected to a single axis actuated with a servomotor that can induce an equivalent tilt in both  $\alpha$  and  $\beta$  to both propellers, *i.e.*,  $n_u = 4 + 2$ . The authors propose a control scheme for trajectory tracking which takes into account the effect of the AAUs' airflow interference. The performance of the platform is demonstrated with a prototype while sliding along a surface.

In (McArthur et al. 2017) the authors present a quadrotor design based on the composition of a  $\Delta$ -trirotor (see section Trirotor (3 AAUs)) with an additional tail propeller tangentially tilted to provide thrust in a lateral direction as shown in Fig. 18. The design is endowed with this extra propeller to help push an object. All propellers in this design are fixed, except for the trirotor tail which is actively tilted radially,  $n_u = 4 + 1$ . The proposed design was implemented in a prototype used to validate the extra push abilities in a planar experiment (APhI.1) without flying; in this experiment, the coplanar/collinear propellers were turned off, and an extra propeller was added to control the yaw just during these experiments.

apparition	$n_u$	DoF	properties	abilities	maturity	variety of figure
R. Mahony et al. 2012   Bouabdallah, Noth, et al. 2004   Bouabdallah and Siegwart 2005	4		UDT	H.2, TT.2, APhI.3	product	
Falanga et al. 2017	4		UDT	H.2, TT.2, APhI.0/APhI.3	prototype	Fig. 11
Ryll et al. 2012   Ryll et al. 2013   Ryll et al. 2015	4+4	$\alpha_1, \alpha_2, \alpha_3, \alpha_4$	OA/OD	H.3, TT.4, APhI.0/APhI.4	prototype	Fig. 11
Falconi and Melchiorri 2012	4+4	$\alpha_1, \alpha_2, \alpha_3, \alpha_4$	OA	H.3, TT.4, APhI.0/APhI.4	simplistic simulation	Fig. 11
Oosedo et al. 2016	4+4	$\alpha_1, \alpha_2, \alpha_3, \alpha_4$	OA	H.3, TT.4, APhI.0/APhI.4	prototype	Fig. 11
Yih 2016	4+4	$\alpha_1, \alpha_2, \alpha_3, \alpha_4$	OA	H.3, TT.4, APhI.0/APhI.4	realistic simulation	Fig. 11
Nemati and Kumar 2014   Nemati, Soni, et al. 2016	4+2	$(\alpha_1, \alpha_3), (\alpha_2, \alpha_4)$	FA	H.3, TT.4, APhI.0/APhI.4	prototype	Fig. 11
Badr et al. 2016	4+4	$\beta_1, \beta_2, \beta_3, \beta_4$	FA	H.3, TT.4, APhI.0/APhI.4	simplistic simulation	Fig. 13
Devlin et al. 2018	4+4	$\beta_1, \beta_2, \beta_3, \beta_4$	OA	H.3 TT.4 APhI.1/APhI.4	prototype	Fig. 13
Scholz et al. 2016	4+2	$(\beta_1, \beta_2), (\beta_3, \beta_4)$	FA	H.3, TT.4, APhI.0/APhI.4	simplistic simulation	Fig. 13
Long, Lyttle, et al. 2012   Long, Gelardos, et al. 2014	4+4 7	$\beta_1, \beta_2, \beta_3$ $\beta_1, \beta_2, \beta_3$	FA	H.3, TT.4, APhI.0/APhI.4	prototype	Fig. 14
Şenkul and Altuğ 2013	1+8	$\alpha_1, \alpha_2, \alpha_3, \alpha_4, \beta_1, \beta_2, \beta_3, \beta_4$	UDT	H.2, TT.2, APhI.0/APhI.3	simplistic simulation	Fig. 15
Şenkul and Altuğ 2014	4+8	$\alpha_1, \alpha_2, \alpha_3, \alpha_4, \beta_1, \beta_2, \beta_3, \beta_4$	OA	H.2, TT.2, APhI.0/APhI.4	simplistic simulation	Fig. 15
Hua et al. 2015   Odelga et al. 2016	4+2	$(\alpha_1, \alpha_2, \alpha_3, \alpha_4), (\beta_1, \beta_2, \beta_3, \beta_4)$	FA	H.4, TT.4, APhI.0/APhI.4	simplistic simulation	Fig. 16
De Martini et al. 2017	4(Bi)+2	$(\alpha_1, \alpha_2, \beta_1, \beta_2), (\alpha_3, \alpha_4, \beta_3, \beta_4)$	FA	H.4, TT.4, APhI.0/APhI.4	simplistic simulation	Fig. 15
Khoo et al. 2017	4+8	$\alpha_1, \alpha_2, \alpha_3, \alpha_4, \beta_1, \beta_2, \beta_3, \beta_4$	OA	H.3, TT.4, APhI.0/APhI.4	prototype	Fig. 15
Segui-Gasco et al. 2014	4+8	$\alpha_1, \alpha_2, \alpha_3, \alpha_4, \beta_1, \beta_2, \beta_3, \beta_4$	OA	H.3, TT.4, APhI.0/APhI.4	prototype	Fig. 15
Kawasaki et al. 2015	4+2	$(\alpha_1, \alpha_3, \beta_1, \beta_3), (\alpha_2, \alpha_4, \beta_2, \beta_4)$	MDT	H.3, TT.3, APhI.1/APhI.4	prototype	Fig. 17
McArthur et al. 2017	4+1	$\alpha_1$	MDT	H.2, TT.2, APhI.1/APhI.3	prototype (partially tested)	Fig. 18

TABLE VIII: Recapitulative table for the quadrotors ( $N = 4$ ).

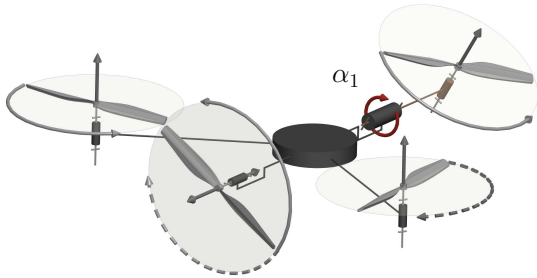


Fig. 18: Conceptual 3D kinematic representation of a quadrotor with propellers tilting/tilted radially/tangentially as presented in (McArthur et al. 2017).

While the quadrotor design was exploited extensively in the literature and allowed platforms to reach OA/OD, the limited number of propellers does not allow the platforms to exhibit more than UDT and **H.2** without any servomotors. While quadrotors are still very popular, many papers from the literature exploit designs with  $N > 4$  to exploit actuation properties higher than UDT, especially for applications of APhI, where lateral forces are often required.

## VII. PENTAROTOR (5 AAUs)

The case of  $N = 5$  AAUs is not commonly found in the literature, due to its lack of symmetry implied by the odd number of AAUs. Usually, symmetric designs are favored thanks to their ease of control and diagonal Inertia matrix.

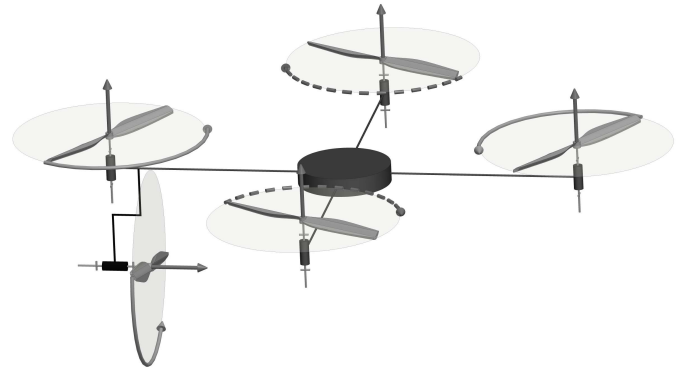


Fig. 19: Conceptual 3D kinematic representation of the pentarotor design presented in (Albers et al. 2010).

The only documented non-coplanar/collinear pentarotor design we could find is introduced in (Albers et al. 2010) and can be described as a classical coplanar quadrotor with the addition of a propeller oriented in an orthogonal direction to provide extra actuation for attaining the considered tasks; a conceptual design sketch is shown in Fig. 19, and the design properties and abilities are listed in Tab. IX. The goal is to be able to easily apply a normal force on a wall for tasks such as inspection, cleaning, and painting. All the AAUs orientations are fixed, thus  $n_u = 5$ . Because of its composition design it holds the same properties as classical coplanar quadrotor, plus the ability to push along one extra translational direction. The proposed design was tested on a prototype, and its  $\mathfrak{F}_1$  space is presented in Fig. 20.

## VIII. HEXAROTOR (6 AAUs)

A Hexarotor design has  $N = 6$ . For Hexarotors, we can group Coplanar/collinear designs into two groups, star-shaped

apparition	$n_u$	properties	abilities	maturity	figure
Albers et al. 2010	5	MDT	H.3, TT.3, APhI.1/APhI.3	prototype (APhI.1)	Fig. 19

TABLE IX: Recapitulative table for the pentarotors ( $N = 5$ ).

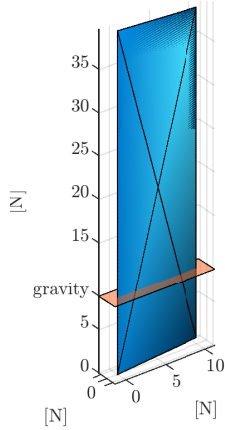


Fig. 20: visualization of the  $\mathfrak{F}_1$  space of the design presented in (Albers et al. 2010) in blue, and the corresponding gravity plane in orange. The design consists of a quadrotor with an additional propeller pointing in a lateral direction. All propellers are fixed.  $N = 5$  and  $n_u = 5$ . Profile: subsurface of the  $xz$ -plane, where we assume the 5th propeller is pointing in the  $x$ -direction. The surface has the largest height for  $x = 0$  and decreases as  $x$  increases.

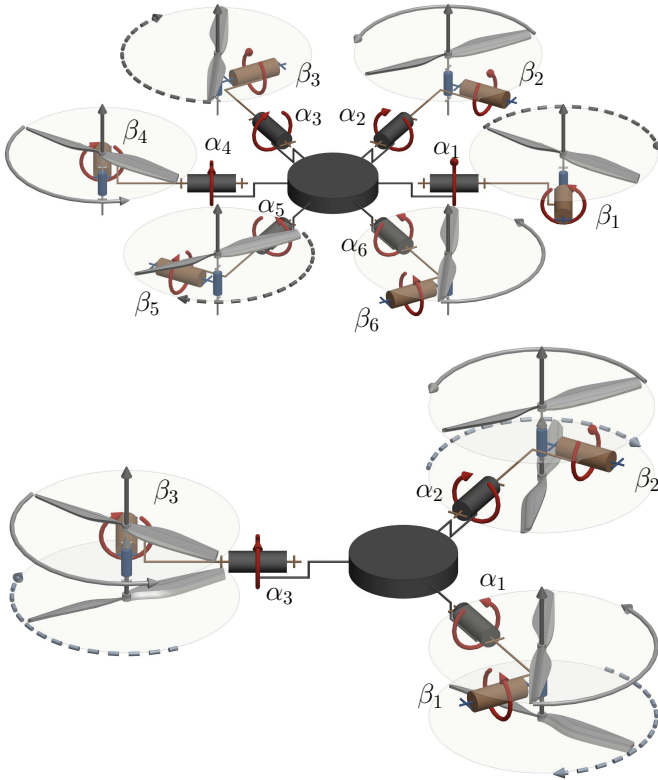


Fig. 21: Conceptual 3D kinematic representation of (top) star-shaped hexarotor, (bottom) Y-shaped hexarotor with propellers tilting/tilted in  $S^2$ .

and Y-shaped as shown in Fig. 21 top and bottom respectively. The former refers to a distribution where each AAU is a vertex of the star, while the latter considers a disposition similar to the delta trirotor. The system properties and capabilities are the same as for the coplanar/collinear quadrotor, except that the Y-shaped hexarotor is robust to AAU failure, while the star-shaped is not, see (Michieletto et al. 2017).

As for hexarotors with tilted AAUs, tilting angles can be chosen so as  $\mathbf{F}$  is full rank, and thus the platform is fully actuated. In fact, this is the minimal configuration for which it is possible to obtain FA of the 6D pose without any dynamic tilting of the propellers. However, as the AAUs are tilted, part of the energy is dissipated internally to balance the platform while hovering; as such, tilt-angles have to be chosen as a trade-off between propulsive efficiency (*i.e.*, closer to coplanar/collinear) and maneuverability in the sense of decoupling between actuation force and moment. This choice can be made either based on heuristics or by optimizing a cost function specific to the application at hand. The impact of both radial and tangential tilting, in the case of unidirectional fixed-tilt AAUs for hexarotor, is formally studied in (Michieletto et al. 2017). It appears that a sufficient condition to ensure full-rankness of  $\mathbf{F}$  is to have non-null tangential tilting even in the absence of radial tilting. However, if the tangential tilting is small enough,  $\mathbf{F}$  is close to loose full-rankness, *i.e.*, has a large condition number, and if the tilting is too important internal forces augment and the design loses energy efficiency. To alleviate that effect, radial tilting can be introduced as a way to lower the condition number for small tangential tilting. It is also proven that hexarotors, for which AAUs are only radially tilted, are *fully vulnerable* to AAU failure.

As most of the hexarotor designs found in the literature consider unidirectional fixed-tilt AAUs, thus obtaining  $n_u = 6$ , in what follows AAUs are assumed to have a fixed-tilt unless specified otherwise. Table X summarizes the properties and abilities of the hexarotor designs reviewed below.

#### A. Radial Tilting Designs

In (Jiang and Voyles 2014) (and previous work) the design focuses on allowing *force closure*, *i.e.*, the ability to instantaneously resist 6D wrench perturbation such as wind while in contact with the environment. To obtain such a design, AAUs are radially tilted by a constant angle of  $20^\circ$ , obtained considering a manipulability index (Yoshikawa 1985); the design is tested on a prototype. The  $\mathfrak{F}_1$  space of similar designs is shown in Fig. 22.

On the other hand, authors of (Ryll, Bicego, et al. 2016) present a design called *FastHex* where AAUs' radial tilting can be changed simultaneously with a single servomotor for all AAUs as shown in Fig. 23, thus obtaining  $n_u = 6 + 1$ . This allows switching between UDT and FA configurations of the multirotor with only one additional input. This design can be

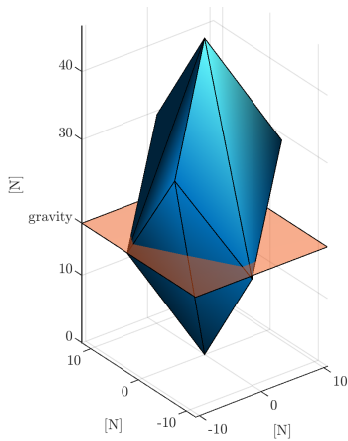


Fig. 22: visualization of the  $\mathfrak{F}_1$  space of a hexarotor with propellers equally tilted about a fixed  $\alpha$  angle. The corresponding gravity plane is shown in orange.  $N = 6$  and  $n_u = 6$ . Profile description: trigonal trapezohedron.

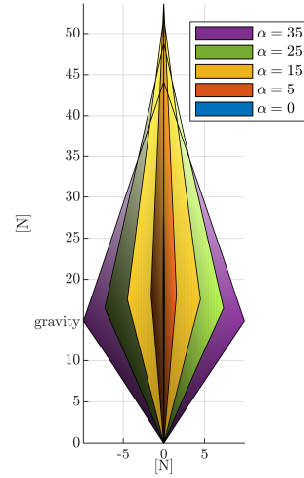


Fig. 24: visualization of a cross-section of the  $\mathfrak{F}_1$  space of the *FastHex* design at different propeller tilts  $\alpha$ . The  $\mathfrak{F}_1$  space is similar to coplanar/collinear design for  $\alpha=0$ ; as  $\alpha$  increases, the platform is capable of applying further lateral forces while decreasing the possible lift.

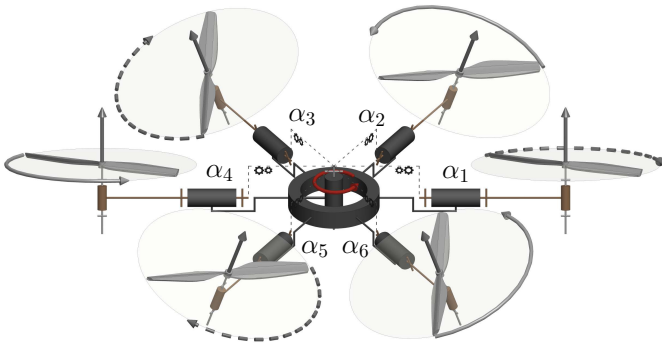


Fig. 23: Conceptual 3D kinematic representation of the *FastHex* design presented in (Ryll, Bicego, et al. 2016). The propellers are tilting radially. Highlighted the locked tilting that forces all the propellers to tilt of the same angle  $\alpha$ .

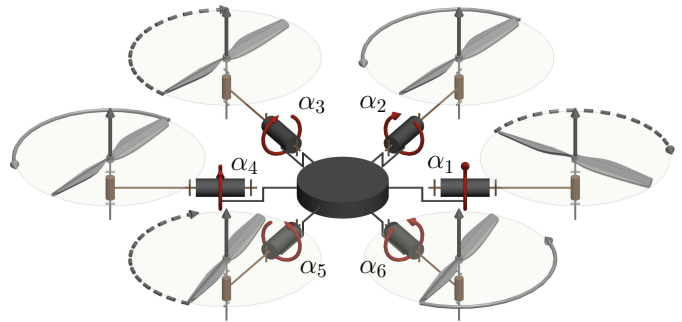


Fig. 25: Conceptual 3D kinematic representation of the *Voliro* design presented in (Kamel et al. 2018) and (Elkhatib 2017). The propellers are tilting radially and all independently.

used to optimize between energy efficiency during free-flight (coplanar/collinear AAUs) and an adequate force/moment decoupling during physical interactions. Figure 24 illustrates the different possible  $\mathfrak{F}_1$  spaces at different tilts. Extensive simulations validate the benefits of such a design for a real case scenario, while later Bicego 2019 also validates these results in real-world experiments.

In (Kamel et al. 2018) and (Elkhatib 2017), each AAU is equipped with a servomotor (6 in total) to tilt independently, thus obtaining  $n_u = 6 + 6$ . The design, named *Voliro*, was tested on a prototype showing successful omnidirectional flights and is shown in Fig. 25.

### B. Tangential Tilting Designs

Differently from the designs in Radial Tilting Designs, Giribet et al. 2016 propose a design where the AAUs are tangentially tilted, at a magnitude chosen heuristically at  $\beta = 13^\circ$ . Authors have demonstrated the ability of a vehicle with small tilting to be able to face failure in one of its propellers. Trajectory tracking of the platform was validated through simulation with noise and rotor failure.

In (Pose et al. 2017) the authors also propose a design relying on tangentially tilted AAUs, where the tilting angle is heuristically chosen in a range that ensures the robustness of the design to failures, at a fixed  $\beta = 17^\circ$  for all AAUs. The controller does not exploit the MDT property of the design and focuses on emulating the behavior of coplanar design, by only considering a reduced output vector and finding optimal control allocation to the spinning velocity of the most solicited AAU. This design is shown to be robust to single AAU failure through experiments on a prototype of the design.

The above two designs are mechanically equivalent despite the different choice of tilt angle  $\beta$ , however, the controlled output of each is different, with (Pose et al. 2017) not fully exploiting the FA property.

Another design is proposed in (S.-Guerrero and R.-Torres 2018), where the authors combine a hexarotor with a hexapod design, mounting each propeller on one of the platform's legs, which can rotate about two axes corresponding to the propeller's arrangement about the center of mass, and the propeller's tangential tilt. The platform is able to crawl and fly, and hence it's name *hexapodopter*. The authors prove that

apparition	$n_u$	DoF	properties	abilities	maturity	variant of figure
Jiang and Voyles 2014	6		FA	H.3, TT.4, APhI.0/APhI.4	prototype	Fig. 21(top)
Ryll, Bicego, et al. 2016	6+1	$(\alpha_1, \alpha_2, \alpha_3, \alpha_4, \alpha_5, \alpha_6)$	FA	H.3, TT.4, APhI.0/APhI.4	realistic simulation	Fig. 23
Bicego 2019					prototype	
Kamel et al. 2018   Elkhatab 2017	6+6	$\alpha_1, \alpha_2, \alpha_3, \alpha_4, \alpha_5, \alpha_6$	OD	H.4, TT.4, APhI.0	prototype	Fig. 25
Giribet et al. 2016   Pose et al. 2017	6		FA	H.3, TT.4, APhI.0/APhI.4	realistic simulation	Fig. 21(top)
S.-Guerrero and R.-Torres 2018	6+6	$\beta_1, \beta_2, \beta_3, \beta_4, \beta_5, \beta_6$	OA	H.3, TT.4, APhI.1/APhI.4	simplistic simulation	Fig. 21(top)
Crowther et al. 2011	6+1	$(\alpha_1, \alpha_2, \alpha_5, \alpha_6, \beta_1, \beta_2, \beta_5, \beta_6)$	OA	H.3, TT.4, APhI.0/APhI.4	prototype	Fig. 21(top)
Ryll, Muscio, et al. 2017	6		FA	H.3, TT.4, APhI.1/APhI.4	prototype	Fig. 21(top)
Staub et al. 2018	6		FA	H.3, TT.4, APhI.4	prototype	Fig. 21(top)
Rajappa et al. 2015	6		FA	H.3, TT.4, APhI.0/APhI.4	simplistic simulation	Fig. 21(top)
Morbidi et al. 2018	6+2	$(\alpha_1, \alpha_2, \alpha_3, \alpha_4, \alpha_5, \alpha_6, \beta_1, \beta_2, \beta_3, \beta_4, \beta_5, \beta_6)$	OA	H.3, TT.4, APhI.0/APhI.4	simplistic simulation	Fig. 23
Rashad, Kuipers, et al. 2017	6(Bi)		OD	H.4, TT.4, APhI.0/APhI.4	realistic simulation	Fig. 21(top)
Rashad, Engelen, et al. 2019	6		FA	H.3, TT.4, APhI.1/APhI.4	prototype	Fig. 21(top)
Myeong et al. 2019	6+1	$(\alpha_1, \alpha_2, \beta_1, \beta_2)$	OA	H.3, TT.4, APhI.1/APhI.4	prototype	Fig. 21(bottom)

TABLE X: Recapitulative table for the hexarotors ( $N = 6$ ).

their design can achieve FA, and assess their design through simulation.

### C. $S^2$ Tilting Designs

Crowther et al. 2011 present a hexarotor design where each AAU is allowed to tilt in  $S^2$ . Crowther et al. 2011 describe designs constrained such that the thrusts produced by each pair of AAUs are aligned along 3 orthogonal directions, possible AAUs' orientations and direction are further grouped in 3 classes. The authors validate their feedback linearization based controller in a static experiment on a prototype of one of the detailed classes. This enforced orthogonality ensures that each 6D translation is actuated by a single AAU which comes at the logical corollary cost that each AAU should be able to sustain the full weight of the design. The authors also compare their design to a coplanar design which maximizes propulsive efficiency

Conversely, the following works consider the tilting of the AAUs in a more general way, *i.e.*, not enforcing orthogonality of the individual thrusts. In addition, we note that most works considering generic AAUs orientation in  $S^2$ , are interested to find the optimal AAUs orientations and thus consider both radial and tangential tilting in their optimization problem formulation, even if the resultant optimal orientation doesn't always comprise both tiltings.

Another design is proposed in (Mehmood et al. 2016), where the tilt angles about  $S^2$  are chosen to optimize maneuverability, defined as the max acceleration reached in a given direction. The paper also investigates the failure of a single propeller and concludes with theoretical contributions.

In (Tadokoro et al. 2017) optimal design based on 'dynamic manipulability measure' is investigated. It can be understood as omnidirectional acceleration capabilities similar to the manipulator case and is expressed as  $\sqrt{\det \mathbf{F}\mathbf{F}^T}$ . This work also proves that it is sufficient to study the planar disposition of the AAUs, as any spatial distribution can be brought to its equivalent plane form (neglecting some mass/inertia changes, and not taking aerodynamic cross-wind into account).

Both methods rely on heavy symmetry constraints imposed on the design, in terms of AAU disposition and tilting.

Interestingly the optimal design for these two metrics does not require AAUs to be oriented in  $S^2$ , only radial tilting of around  $37^\circ$  and  $35^\circ$  respectively for (Mehmood et al. 2016) and (Tadokoro et al. 2017). However, we do note that only radial tilting renders the design *fully vulnerable* to AAU failure, (Micheletto et al. 2017).

The aforementioned maxima are also acknowledged in (Rajappa et al. 2015), where the AAUs tilting are adjusted before flight such as to minimize the norm of the control effort upon the desired trajectory. Indeed, it is important to underline that the optimal value of the tilt angles highly depends on the specific trajectory that the UAV has to perform. The problem has been solved searching for an optimal arrangement with respect to a minimum control effort over a desired trajectory. In the end, a feedback linearization technique has been also exploited.

In (Ryll, Muscio, et al. 2017) a design to enable physical interaction is described. AAUs are tilted symmetrically to guarantee a trade-off between maximum lateral forces and losses due to internal forces, the magnitude of the tilting angles are respectively  $30^\circ$  and  $10^\circ$ . The control law is based on an outer-loop admittance control and an inner loop full-pose geometric controller. Moreover, the interaction forces are estimated by a wrench observer. The effectiveness of the theoretical results has been also tested in real experiments.

Staub et al. 2018 propose a design, called *OTHex*, tailored to the special case of cooperative beam manipulation. This design is similar to (Ryll, Muscio, et al. 2017), where the AAUs are tilted of fixed angles to allow FA of the multirotor, this is important for cooperative manipulation as it allows the multirotor to resist lateral disturbances without the need for reorienting as in the coplanar case. The OTHex design also considers an AAU distribution less symmetric than (Ryll, Muscio, et al. 2017), allowing a beam to pass through the propellers' volume.

The work by Morbidi et al. 2018 presents a platform design where the tilting of all propellers is synchronized so as all propellers tilt about the same radial and tangential angles. Their study can be applied for designs with active or passive tilting, thus  $n_u = 6 + 2$ . The authors determined a minimum-

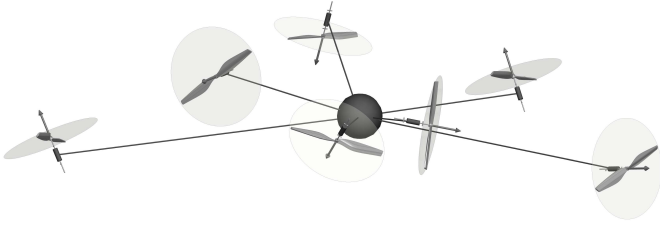


Fig. 26: Conceptual 3D kinematic representation of the heptarotor design presented in (Nikou et al. 2015).

energy trajectory between two predefined boundary states and to achieve this goal an optimal control has been used by including also the dynamics of the brushless DC motors. Moreover, a deep analysis of the singularities of the allocation matrix has been presented. The tilting angles  $(\alpha, \beta)$  come from a high-level tilt planner which is pre-computed offline and is known by the optimizer. In some sense, this work is the opposite of (Rajappa et al. 2015) where optimal tilt-angles were found to follow a pre-computed trajectory.

The two next works consider bidirectional AAUs. In (Rashad, Kuipers, et al. 2017) a design aimed at maximizing actuation wrench is proposed while considering bidirectional AAUs. This leads to a OD design that has been validated in simulation with external wrench disturbances. The wrench maximization also results in only radial tilting. Their design was later demonstrated on a prototype with **APhI.1** capabilities in (Rashad, Engelen, et al. 2019), however, with unidirectional propellers.

Myeong et al. 2019 also demonstrate a prototype hexarotor, with the propellers being placed in Y-formation. In their design, two of the motor pairs are placed along a horizontal shaft and can rotate independently in pairs thus obtaining  $n_u = 6 + 1$ . The design is similar to a T-shaped tritorotor with each shaft containing two propellers rotating in opposite to produce zero moment. The platform is endowed with a mechanism that allows it to apply a force on walls to aid in their inspection.

### IX. HEPTAROTOR (7 AAUs)

This case is of particular interest because for designs that have AAUs with fixed orientation (*i.e.*,  $n_u = N$ ) and all unidirectional thrust propellers, the condition  $N \geq 7$  is necessary to achieve OD as proven in (Tognon and Franchi 2018). Despite its OA/OD ability with fixed AAUs, the design is not popular and only two such designs have been found in the literature.

Arguably, heptarotor designs first appeared in Nikou et al. 2015, where an optimal design for manipulation task with body-fixed end-effector is considered, see Fig. 26. The unidirectional AAUs constraint is explicitly considered. The optimization considers the condition number of  $\mathbf{F}$  to ensure that the wrench produced is not sensitive to small deviations of the AAUs generated thrust. Additionally, the aerodynamic interaction between the AAUs' airflow is considered, and sought to be minimized while keeping the total design volume reasonable. This design is evaluated in a simulation of

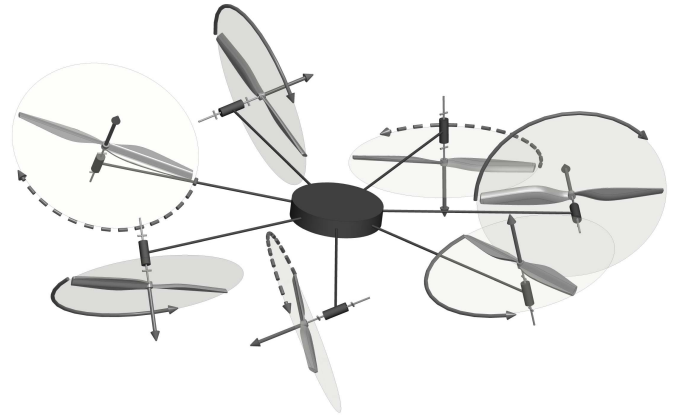


Fig. 27: Conceptual 3D kinematic representation of the heptarotor design presented in (Tognon and Franchi 2018).

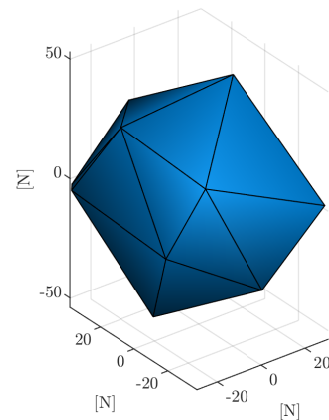


Fig. 28: visualization of the  $\mathfrak{F}_1$  space of the design presented in (Tognon and Franchi 2018). The design consists of a heptarotor with fixed unidirectional propellers, with orientations designed to allow omnidirectional flight.  $N = 7$  and  $n_u = 7$ . Profile description: irregular icositetrahedron contained inside a sphere in  $\mathbb{R}^3$ .

trajectory tracking, in non-hovering orientation, subjected to disturbances and controlled via a backstepping approach.

In (Tognon and Franchi 2018) the optimization design problem assumes fixed positions of the AAUs, radially around the CoM, and optimize their respective tilting. A major design criterion considered is a minimum allocation-matrix condition number, which aims at an equal sharing of the effort needed to generate wrenches in any direction. Additionally, the notion of ‘balanced design’ is introduced which guarantees an equal sharing of the extra effort needed to keep all AAUs’ individual thrust positive. An associated controller relying on model inversion and PID is proposed alongside. The general optimal design problem is proposed to make the design OD while minimizing the range of required control inputs to hover in any orientation. It is described and applied for  $N = 7$ , with an extensive realistic simulation of trajectory tracking, with several non-idealities described in the corresponding technical report. The authors hint that minimizing the condition number of  $\mathbf{F}$ ,  $\kappa(\mathbf{F})$ , for a balanced design, minimizes the norm of the input. The result of this optimization for  $N = 7$  is shown in Fig. 27. The  $\mathfrak{F}_1$  set of this design is presented in Fig. 28.

apparition	$n_u$	properties	abilities	maturity	figure
Nikou et al. 2015	7	OA, FA	H.4, TT.4, APhI.4	realistic simulation (TT.4)	Fig. 26
Tognon and Franchi 2018	7	OA, OD	H.4, TT.4, APhI.0/APhI.4	realistic simulation (TT.4)	Fig. 27

TABLE XI: Recapitulative table for the heptarotors ( $N = 7$ ).

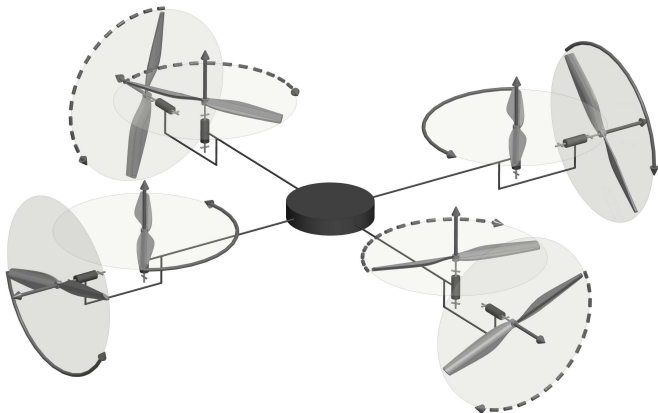


Fig. 29: Conceptual 3D kinematic representation of the octorotor design presented in (Romero et al. 2007).

#### X. OTHER DESIGNS WITH 8 AAUS OR MORE

We group all other platforms with  $N \geq 8$  together, where we note that the majority of such designs consist of octorotors. Some notable exceptions are the commercial ‘heavy lifter’, which are coplanar/collinear multirotor designs. Examples are the (Inc. 2016) with  $N = 14$ , and *Volocopter*<sup>5</sup> with  $N = 18$ .

The preference of the octorotor design over others in the literature can be explained by the favored symmetric multirotor design with an even number of propellers. Moreover, due to the required compactness of commercial platforms, it becomes important for the design to have the least number of propellers for the given application. A larger number of propellers adds more weight to the platform and requires a larger platform to avoid aerodynamic interactions between adjacent AAUs.

##### A. Enhanced Quadrotor design

Octorotor designs in this section can be seen as an attempt to overcome the translational under-actuation of coplanar/collinear quadrotors, by adding 4 AAUs with thrust oriented in the non-actuated directions, similarly to the pentarotor in (Albers et al. 2010).

In (Romero et al. 2007), a multirotor design based on a quadrotor design is proposed with four additional smaller AAUs, orthogonal to the four main ones. A conceptual kinematic design is shown in Fig. 29. The extra AAUs are devoted to controlling the lateral motion of the multirotor. It is interesting to note that the lateral smaller propellers produce an airflow that perturbs the induced wind speed in the main propellers increasing its lift. This term is compensated by a feedforward linearization of the aerodynamics interaction to obtain a full decoupling between the rotational and translational movements. The trajectory tracking problem is then

<sup>5</sup>www.volocopter.com

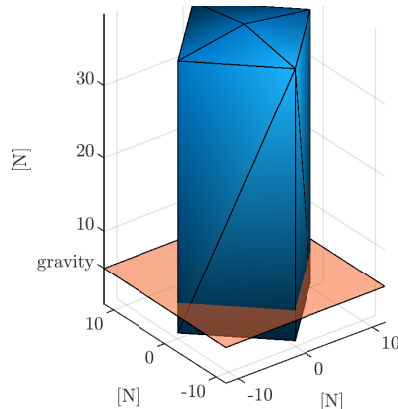


Fig. 30: visualization of the  $\mathfrak{F}_1$  space of the design presented in (Romero et al. 2007). The corresponding gravity plane is shown in orange. The design consists of 8 propellers, with 4 being collinear/coplanar with thrust pointing upwards to provide lift, and the other 4 pointing in the positive and negative  $x$  and  $y$  direction respectively.  $N = 8$  and  $n_u = 8$ . Profile description: cuboid with square pyramid on top.

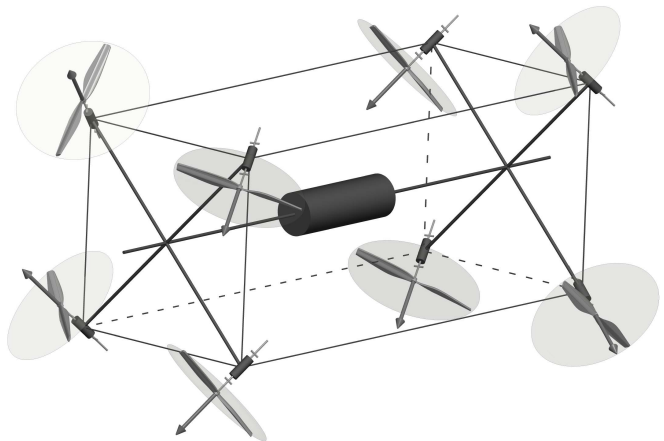


Fig. 31: Conceptual 3D kinematic representation of the octorotor design presented in (Park, Her, et al. 2016; Park, Lee, et al. 2018).

solved by resorting to a mixture of a model-independent PD controller, coupled with a model-dependent compensation of the Coriolis and gyroscopic nonlinear torques. The  $\mathfrak{F}_1$  space of this design is presented in Fig. 30.

In (Fu et al. 2017) the AAUs are also tilted in the lateral plane but are located differently, reducing the cross-wind which improved the efficiency; this results again in an FA design.

##### B. Optimized Octorotor Designs

Following these basic octorotor designs, some more refined designs can be found in the literature.

apparition	$n_u$	properties	abilities	maturity	figure
Romero et al. 2007Fu et al. 2017	8	OA, OD	H.4, TT.4, APhI.0/APhI.4	prototype	Fig. 29
Park, Lee, et al. 2018	8	OD	H.4, TT.4, APhI.0/APhI.4	prototype	Fig. 31
Brescianini and D'Andrea 2016	8(Bi)	OA, OD	H.4, TT.4, APhI.0/APhI.4	prototype	Fig. 32

TABLE XII: Recapitulative table for the octorotors and the platforms with more than 8 rotors  $N \geq 8$ .

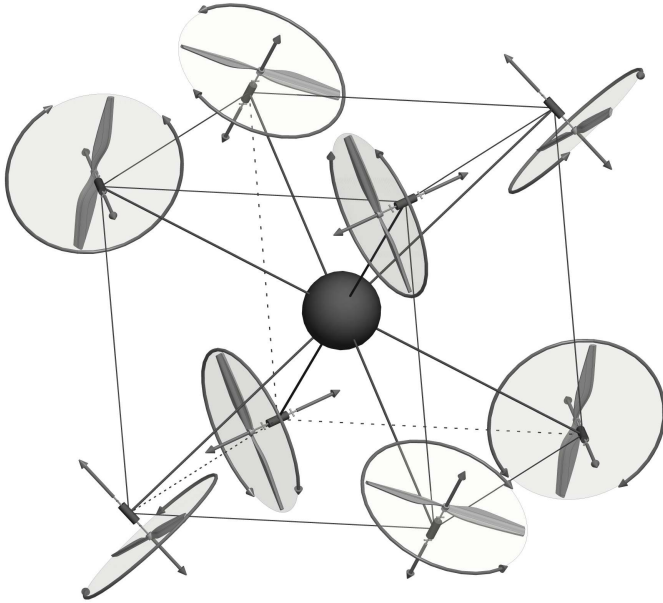


Fig. 32: Conceptual 3D kinematic representation of the OD octorotor design presented in (Brescianini and D'Andrea 2016).

In (Park, Her, et al. 2016; Park, Lee, et al. 2018) aerodynamic interferences are included in the optimization problem. The goal of the optimization is to find an optimal wrench generation and an optimal rotor location within a maximum allowable volume. The first design was presented in (Park, Her, et al. 2016) with  $N = 6$ , and then a similar design was presented later in (Park, Lee, et al. 2018) with  $N = 8$ . The final design consists of a longitudinal bar along which propellers are placed in fixed nonsymmetric positions as shown in Fig. 31 showing the case with  $N = 8$ , with  $n_u = N$ . Eventually, a PID (system-independent) control strategy is implemented. In this case, to obtain bidirectional propulsion, two unidirectional propellers have been stacked together in opposite directions.

An optimized octorotor design with bidirectional propellers is presented in (Brescianini and D'Andrea 2016) and shown in Fig. 32. The platform is intended to be omnidirectional, and was designed by placing propellers on the edges of an octahedron to have a rotational invariant inertia tensor. Then the rotor disk orientations were chosen to maximize a measure of the platform's agility, *i.e.*, the norm of the maximum attainable force-torque in any direction. As the system is FA, the authors exploit the feedback linearization technique to derive the controller.

Finally, in the technical report attached to Tognon and Franchi 2018, which has been introduced in the previous section, an application for  $N = 8$  unidirectional propellers is briefly introduced to show the generality of the described

design method for fixed unidirectional AAUs.

## XI. DISCUSSION

Throughout the review, we realized a few patterns in the presented designs, such as 1) the focus on symmetrical designs, 2) the use of uni-directional propellers, 3) ignoring aerodynamic interaction between propellers, 4) and finally system modeling not considering actuation limits.

While these patterns are prevalent, there has been some attempts in the literature to break these renditions. However, the full analysis of each, the corresponding advantages, and their incorporation in future designs is still to be done.

### A. Platform Symmetry

We can see that in the presented literature, the majority of designs enforce some symmetry assumptions. These symmetries vary from placing all propellers on a horizontal axis; assuming the same tilt for all propellers (with varying directions); assuming all propellers to be placed on a circumference around the geometric center of the platform, or finally having an even number of propellers. The symmetry is usually done to simplify the mechanical design and the resulting modeling and control, which in turn results in stable platforms and easy to mass-produce designs. However, we have seen that Tognon and Franchi 2018 by optimizing the tilt of the propellers about the horizontal axis, independently of any symmetry between the tilts, was able to achieve OD with  $N \geq 7$ . Conversely, Brescianini and D'Andrea 2016 achieved OD with a design where the propellers are no longer placed on a horizontal axis, but rather on the vertices of an octahedron. Finally, Nikou et al. 2015 removed any symmetry assumption and optimized the location and orientation of all propellers for a given application. As such, we can see that the relaxation of symmetric heuristics, combined with an optimization of the platform based on performance metrics can achieve a wider allocation space, and advance multirotor designs beyond what is currently possible.

### B. Bi-directional propellers

We realized throughout the review that the use of bidirectional propellers is scarce, where only a few designs (De Martini et al. 2017; Rashad, Kuipers, et al. 2017; Park, Her, et al. 2016; Park, Lee, et al. 2018) and (Brescianini and D'Andrea 2016)) decided to use such propellers, with the benefit of controlling the flow of a propeller in any direction. This can be related to the 'singularity' near the zero-thrust region (Park, Lee, et al. 2018), where the propeller has a deadband, followed by a high slope region. Moreover, hardware solutions for bidirectional thrust AAUs, either reversible ESCs or variable pitch propellers, are not satisfactory to fully exploit them in

multirotor designs. Commercial solutions for reversible ESCs are scarce and the geometry of the propeller is less energy efficient than the unidirectional counterpart. Lastly, at low speed, the controllability of the exerted forces is very low, *i.e.*, unsatisfactory for practical uses. The variable pitch propeller can mitigate some of these issues but they come at the expense of additional mechanical complexity and weight, which is also not very practical. Another solution that can be achieved in this part is the use of bidirectional propellers while avoiding the allocation near the inversion zone of each propeller, however, proper optimization software must be designed for this regards, in addition to the need for a redundancy in the allocation capabilities to be able to achieve required allocation in such cases.

### C. Aerodynamic Interaction between Propellers

The field at large could benefit from further studies on the aerodynamic effects at play, especially the interplay between AAUs cross-wind. The integration of the aerodynamic effects in the model used for control synthesis should permit feed-forward cancellation of these effects. This is of particular importance for the development of platforms endowed with fine force interaction capabilities. Also, a good model of the aerodynamic effects could be leveraged in the design process, extending (Nikou et al. 2015) and (Park, Lee, et al. 2018), or benefiting from (Waslander and Wang 2009).

### D. Actuator Limits

Actuator saturation is often dismissed in theoretical studies but plays an important role in practice. Indeed, saturations hinder the multirotor dynamics, and if not taken into account properly, can result in destabilizing the control actions, in particular in dynamical maneuvers or while in physical interaction. While a few papers study the saturation's effect on control (Franchi et al. 2018; Invernizzi and Lovera 2017), we didn't find papers that include these saturations in the platform design.

## XII. CONCLUSION

In this literature review of multirotor design, we first proposed a universal parametrization of multirotors in order to try to homogenize the vast literature on the topic. Based on this parametrization we first proposed a set of system properties and system capabilities for multirotors. Then we evaluated the vast literature on multirotor design and highlighted key conditions to reach certain properties. Finally, we grouped the reviewed designs into classes based on their number of AAUs as we found it more natural for the readers, and showed how designs from each class expanded the allocation capabilities of such class. To the authors' knowledge, this literature review is the first of its kind, and encompasses most of the relevant designs on the topic.

From this literature review and the proposed taxonomy, we could see that initial designs started as a method to upgrade a classical helicopter aircraft (*i.e.*, a birotor, with one variable pitch main rotor with a cyclic input on one axis, and one

perpendicular in the tail), then either the design degenerated the platform to push the aerodynamics of the design to have flight with the least number of controls, or increased the number of actuators and changed their disposition about the CoM of the platform to achieve more stable platforms (quadrotors), or achieve higher levels of actuation (MDT, FA, OA, OD). Eventually, coplanar/collinear quadrotors became the base case for most designs thanks to their availability, stability, and the simplicity of their mechanical design.

The changes from classical designs entailed advantages in allocation and allowed the platforms to be able to interact with the environment, resist disturbances, apply lateral forces without a change in direction, and become robust to AAU failures. In our summary of each platform, we showed how each design corresponded to a specific set of abilities and properties. Recent platform designs started shifting more towards achieving omnidirectional flights, or decoupled force-moment allocation, preferred for physical aerial manipulation tasks, with this last application increasing in popularity thanks to the technological impact it entails.

## REFERENCES

- Albers, A., S. Trautmann, T. Howard, T. A. Nguyen, M. Frietsch, and C. Sauter (2010). "Semi-autonomous flying robot for physical interaction with environment". In: *2010 IEEE Conference on Robotics, Automation and Mechatronics*, pp. 441–446.
- Amiri, N., A. Ramirez-Serrano, and R. Davies (2011). "Modelling of opposed lateral and longitudinal tilting dual-fan unmanned aerial vehicle". In: *IFAC Proceedings Volumes 44.1*, pp. 2054–2059.
- Anzai, T., M. Zhao, X. Chen, F. Shi, K. Kawasaki, K. Okada, and M. Inaba (2017). "Multilinked multirotor with internal communication system for multiple objects transportation based on form optimization method". In: *2017 IEEE/RSJ Int. Conf. on Intelligent Robots and Systems*. Vancouver, Canada, pp. 5977–5984.
- Badr, S., O. Mehrez, and A. E. Kabeel (2016). "A novel modification for a quadrotor design". In: *2016 Int. Conf. on Unmanned Aircraft Systems*. Arlington, VA, USA, pp. 702–710.
- Bicego, D. (2019). "Design and Control of Multi-Directional Thrust Multi-Rotor Aerial Vehicles with applications to Aerial Physical Interaction Tasks". Ph.D. thesis. Université de Toulouse.
- Blouin, C. and E. Lanteigne (2014). "Pitch control of an Oblique Active Tilting bi-rotor". In: *2014 Int. Conf. on Unmanned Aircraft Systems*. Orlando, FL, USA, pp. 791–799.
- Bouabdallah, S., A. Noth, and R. Siegwart (2004). "PID vs LQ control techniques applied to an indoor micro quadrotor". In: *2004 IEEE/RSJ Int. Conf. on Intelligent Robots and Systems*. Sendai, Japan, pp. 2451–2456.
- Bouabdallah, S. and R. Siegwart (2005). "Backstepping and sliding-mode techniques applied to an indoor micro quadrotor". In: *2005 IEEE Int. Conf. on Robotics and Automation*. Barcelona, Spain, pp. 2247–2252.
- Brescianini, D. and R. D'Andrea (2016). "Design, modeling and control of an omni-directional aerial vehicle". In: *2016 IEEE Int. Conf. on Robotics and Automation*. Stockholm, Sweden, pp. 3261–3266.
- Bronz, M., E. J. Smeur, H. Garcia de Marina, and G. Hattenberger (2017). "Development of A Fixed-Wing mini UAV with Transitioning Flight Capability". In: *35th AIAA Applied Aerodynamics Conference*.
- Byrd, R. H., J. C. Gilbert, and J. Nocedal (2000). "A trust region method based on interior point techniques for nonlinear programming". In: *Mathematical programming* 89.1, pp. 149–185.

- Cardoso, D. N., G. V. Raffo, and S. Esteban (2016). “A robust adaptive mixing control for improved forward flight of a tilt-rotor UAV”. In: *2016 IEEE 19th International Conference on Intelligent Transportation Systems (ITSC)*. Rio de Janeiro, Brazil, pp. 1432–1437.
- Chowdhury, A. B., A. Kulhare, and G. Raina (2012). “A generalized control method for a Tilt-rotor UAV stabilization”. In: *2012 IEEE International Conference on Cyber Technology in Automation, Control, and Intelligent Systems (CYBER)*. Bangkok, Thailand, pp. 309–314.
- Crowther, B., A. Lanzon, M. Maya-Gonzalez, and D. Langkamp (2011). “Kinematic analysis and control design for a nonplanar multirotor vehicle”. In: *Journal of Guidance, Control, and Dynamics* 34.4, pp. 1157–1171.
- De Martini, D., G. V. Gramazio, A. Bertini, C. Rottenbacher, and T. Facchinetti (2017). “Design and Modeling of a Quadcopter with Double Axis Tilting Rotors”. In: *Unmanned Systems* 5.03, pp. 169–180.
- Devlin, T., R. Dickerhoff, K. Durney, A. Forrest, P. Pansodtee, A. Adabi, and M. Teodorescu (2018). “ElbowQuad: Thrust Vectoring Quadcopter”. In: *2018 AIAA Information Systems-AIAA Infotech@ Aerospace*, p. 0893.
- Donadel, R., G. V. Raffo, and L.B. Becker (2014). “Modeling and control of a tiltrotor uav for path tracking”. In: *IFAC Proceedings Volumes* 47.3, pp. 3839–3844.
- Elkhatib, O. (2017). “Control Allocation of a Tilting Rotor Hexacopter”. B.S. thesis.
- Escareno, J., A. Sanchez, O. Garcia, and R. Lozano (2008). “Triple tilting rotor mini-UAV: Modeling and embedded control of the attitude”. In: *2008 American Control Conference*. Seattle, WA, USA, pp. 3476–3481.
- Falanga, D., E. Mueggler, M. Faessler, and D. Scaramuzza (2017). “Aggressive quadrotor flight through narrow gaps with onboard sensing and computing using active vision”. In: *2017 IEEE Int. Conf. on Robotics and Automation*. Marina Bay Sands, Singapore, pp. 5774–5781.
- Falconi, R. and C. Melchiorri (2012). “Dynamic model and control of an over-actuated quadrotor uav”. In: *IFAC Proceedings Volumes* 45.22, pp. 192–197.
- Franchi, A., R. Carli, D. Bicego, and M. Ryll (2018). “Full-Pose Tracking Control for Aerial Robotic Systems with Laterally-Bounded Input Force”. In: *IEEE Trans. on Robotics* 34.2, pp. 534–541.
- Fu, Z., B. Xiao and J. Yang, C. Wu, and Y. Wei (2017). “Modeling and control of a new multicopter”. In: *2017 36th Chinese Control Conference (CCC)*. Liaoning, China, pp. 6495–6500.
- Giribet, J. I., R. S. Sanchez-Pena, and A. S. Ghersin (2016). “Analysis and design of a tilted rotor hexacopter for fault tolerance”. In: *IEEE Transactions on Aerospace and Electronic Systems* 52.4, pp. 1555–1567.
- Gress, G. R. (2002). “Using dual propellers as gyroscopes for tilt-prop hover control”. In: *2002 Biennial International Powered Lift Conference and Exhibit*, p. 5968.
- Haus, T., M. Orsag, and S. Bogdan (2016). “Design considerations for a large quadrotor with moving mass control”. In: *2016 Int. Conf. on Unmanned Aircraft Systems*. Arlington, VA, USA, pp. 1327–1334.
- (2017). “A concept of a non-tilting multirotor-UAV based on moving mass control”. In: *2017 Int. Conf. on Unmanned Aircraft Systems*. Miami, FL, USA, pp. 1618–1624.
- Hua, M. D., T. Hamel, P. Morin, and C. Samson (2015). “Control of VTOL vehicles with thrust-tilting augmentation”. In: *Automatica* 52, pp. 1–7.
- Inc., Aeronex (2016). *Heavy duty drone for high payload transportation*. URL: [https://www.aeronex.com/eng/drones/delivery\\_drone/](https://www.aeronex.com/eng/drones/delivery_drone/) (visited on 07/11/2018).
- Invernizzi, D. and M. Lovera (2017). “Geometric tracking control of a quadcopter tiltrotor UAV”. In: *IFAC-PapersOnLine* 50.1, pp. 11565–11570.
- Jiang, G. and R. Voyles (2014). “A nonparallel hexrotor UAV with faster response to disturbances for precision position keeping”. In: *2014 IEEE Int. Symp. on Safety, Security and Rescue Robotics*. Toyako-cho, Hokkaido, Japan, pp. 1–5.
- Kamel, M., S. Verling, O. Elkhatib, C. Sprecher, P. Wulkop, Z. Taylor, R. Siegart, and I. Gilitschenski (2018). “The Voliro Omniorientational Hexacopter: An Agile and Maneuverable Tiltable-Rotor Aerial Vehicle”. In: *IEEE Robotics & Automation Magazine* 25.4, pp. 34–44.
- Kastelan, D., M. Konz, and J. Rudolph (2015). “Fully Actuated Tricopter with Pilot-Supporting Control This work is supported in part by the German Research Foundation (DFG) in the framework of project”. In: *IFAC-PapersOnLine* 48.9, pp. 79–84.
- Kataoka, Y., K. Sekiguchi, and M. Sampei (2011). “Nonlinear control and model analysis of tricopter UAV model”. In: *IFAC Proceedings Volumes* 44.1, pp. 10391–10396.
- Kawasaki, K., Y. Motegi, M. Zhao, K. Okada, and M. Inaba (2015). “Dual connected Bi-Copter with new wall trace locomotion feasibility that can fly at arbitrary tilt angle”. In: *2015 IEEE/RSJ Int. Conf. on Intelligent Robots and Systems*. Hamburg, Germany, pp. 524–531.
- Kendoul, F., I. Fantoni, and R. Lozano (2006). “Modeling and control of a small autonomous aircraft having two tilting rotors”. In: *IEEE Trans. on Robotics* 22.6, pp. 1297–1302.
- KG, Festo A.G. & Co. (2016). *FreeMotionHandling*. URL: [https://www.festo.com/net/SupportPortal/Files/443122/50017\\_Brosch\\_FreeMotionHandling\\_en\\_160329\\_lo\\_ES.pdf](https://www.festo.com/net/SupportPortal/Files/443122/50017_Brosch_FreeMotionHandling_en_160329_lo_ES.pdf) (visited on 07/11/2018).
- Khoo, S., M. Norton, J. J. Kumar, J. Yin, X. Yu, T. Macpherson, D. Dowling, and A. Kouzani (2017). “Robust control of novel thrust vectored 3D printed multicopter”. In: *2017 36th Chinese Control Conference (CCC)*. Liaoning, China, pp. 1270–1275.
- Long, Y., A. Gelardos, and D. J. Cappelleri (2014). “A novel micro aerial vehicle design: The evolution of the omnicopter MAV”. In: *ASME 2014 International Design Engineering Technical Conferences and Computers and Information in Engineering Conference*. Buffalo, NY, USA, V05AT08A092.
- Long, Y., S. Lyttle, N. Pagano, and D. J. Cappelleri (2012). “Design and quaternion-based attitude control of the omnicopter mav using feedback linearization”. In: *ASME International Design Engineering Technical Conference (IDETC)*. Chicago, Illinois, USA, pp. 1413–1421.
- Mahony, R., V. Kumar, and P. Corke (2012). “Multirotor Aerial Vehicles: Modeling, Estimation, and Control of Quadrotor”. In: *IEEE Robotics & Automation Magazine* 19.3, pp. 20–32.
- McArthur, D. R., A. B. Chowdhury, and D. J. Cappelleri (2017). “Design of the I-BoomCopter UAV for environmental interaction”. In: *2017 IEEE Int. Conf. on Robotics and Automation*. Singapore, pp. 5209–5214.
- Mehmood, H., T. Nakamura, and E. N. Johnson (2016). “A maneuverability analysis of a novel hexarotor UAV concept”. In: *2016 Int. Conf. on Unmanned Aircraft Systems*. Arlington, VA, USA, pp. 437–446.
- Michieletto, G., M. Ryll, and A. Franchi (2017). “Control of Statically Hoverable Multi-Rotor Aerial Vehicles and Application to Rotor-Failure Robustness for Hexarotors”. In: *2017 IEEE Int. Conf. on Robotics and Automation*. Singapore, pp. 2747–2752.
- (2018). “Fundamental Actuation Properties of Multi-rotors: Force-Moment Decoupling and Fail-safe Robustness”. In: *IEEE Trans. on Robotics* 34.3, pp. 702–715.
- Michini, B., J. Redding, N. K. Ure, M. Cutler, and J. P. How (2011). “Design and flight testing of an autonomous variable-pitch

- quadrotor". In: *2011 IEEE Int. Conf. on Robotics and Automation*. Shanghai, China, pp. 2978–2979.
- Mistler, V., A. Benallegue, and N. K. M'Sirdi (2001). "Exact linearization and noninteracting control of a 4 rotors helicopter via dynamic feedback". In: *10th IEEE Int. Symp. on Robots and Human Interactive Communications*. Bordeaux, Paris, France, pp. 586–593.
- Mohamed, M. K. and A. Lanzon (2012). "Design and control of novel tri-rotor UAV". In: *2012 UKACC International Conference on control (CONTROL)*. Cardiff, United Kingdom, pp. 304–309.
- Morbidi, F., D. Bicego, M. Ryll, and A. Franchi (2018). "Energy-Efficient Trajectory Generation for a Hexarotor with Dual-Tilting Propellers". In: *2018 IEEE/RSJ Int. Conf. on Intelligent Robots and Systems*. Madrid, Spain, pp. 6226–6232.
- Myeong, W., S. Jung, B. Yu, T. Chris, S. Song, and H. Myung (2019). "Development of Wall-climbing Unmanned Aerial Vehicle System for Micro-Inspection of Bridges". In: *2019 IEEE Int. Conf. on Robotics and Automation*. Montreal, Canada.
- Nemati, A. and M. Kumar (2014). "Modeling and control of a single axis tilting quadcopter". In: *2014 American Control Conference*. Portland, OR, USA, pp. 3077–3082.
- Nemati, A., N. Soni, M. Sarim, and M. Kumar (2016). "Design, Fabrication and Control of a Tilt Rotor Quadcopter". In: *2016 ASME Dynamic Systems and Control Conference*. American Society of Mechanical Engineers. Minneapolis, MN, USA, V002T29A005.
- Nikou, A., G. C. Gavridis, and K. J. Kyriakopoulos (2015). "Mechanical design, modelling and control of a novel aerial manipulator". In: *2015 IEEE Int. Conf. on Robotics and Automation*. Seattle, WA, USA, pp. 4698–4703.
- Odelga, M., P. Stegagno, and H. H. Bühlhoff (2016). "A fully actuated quadrotor UAV with a propeller tilting mechanism: Modeling and control". In: *2016 IEEE/ASME Int. Conf. on Advanced Intelligent Mechatronics*. Banff, Alberta, Canada, pp. 306–311.
- Oosodo, A., S. Abiko, S. Narasaki, A. Kuno, A. Konno, and M. Uchiyama (2016). "Large attitude change flight of a quad tilt rotor unmanned aerial vehicle". In: *Advanced Robotics* 30.5, pp. 326–337.
- Oung, R., F. Bourgault, M. Donovan, and R. D'Andrea (2010). "The Distributed Flight Array". In: *2010 IEEE Int. Conf. on Robotics and Automation*. Anchorage, USA, pp. 601–607.
- Papachristos, C., K. Alexis, and A. Tzes (2011). "Design and experimental attitude control of an unmanned tilt-rotor aerial vehicle". In: *2011 Int. Conf. on Robotics*. Tallinn, Estonia, pp. 465–470.
- (2014). "Efficient force exertion for aerial robotic manipulation: Exploiting the thrust-vectoring authority of a tri-tiltrotor uav". In: *2014 IEEE Int. Conf. on Robotics and Automation*. Hong Kong, China, pp. 4500–4505.
- (2016). "Dual-authority thrust-vectoring of a tri-tiltrotor employing model predictive control". In: *Journal of Intelligent & Robotic Systems* 81.3-4, p. 471.
- Papachristos, C. and A. Tzes (2013). "Large object pushing via a direct longitudinally-actuated unmanned tri-tiltrotor". In: *2013 Mediterranean Conf. on Control and Automation*. Crete, Greece, pp. 173–178.
- Park, S., J. Her, J. Kim, and D. Lee (2016). "Design, modeling and control of omni-directional aerial robot". In: *2016 IEEE/RSJ Int. Conf. on Intelligent Robots and Systems*. Daejeon, Korea, pp. 1570–1575.
- Park, S., J. Lee, J. Ahn, M. Kim, J. Her, G. H. Yang, and D. Lee (2018). "ODAR: Aerial Manipulation Platform Enabling Omni-Directional Wrench Generation". In: *IEEE/ASME Transactions on Mechatronics* 23.4, pp. 1907–1918.
- Pose, C. D., J. I. Giribet, and A. S. Ghersin (2017). "Hexacopter fault tolerant actuator allocation analysis for optimal thrust". In: *2017 Int. Conf. on Unmanned Aircraft Systems*. Miami, FL, USA, pp. 663–671.
- Pounds, Paul, Robert Mahony, and Peter Corke (2010). "Modelling and control of a large quadrotor robot". In: *Control Engineering Practice* 18.7, pp. 691–699.
- Pounds, Paul, Robert Mahony, Peter Hynes, and Jonathan M Roberts (2002). "Design of a four-rotor aerial robot". In: *Proceedings of the 2002 Australasian Conference on Robotics and Automation (ACRA 2002)*. Australian Robotics & Automation Association, pp. 145–150.
- Prothin, S. and J.-M. Moschetta (2013). "A Vectoring Thrust Coaxial Rotor for Micro Air Vehicle: Modeling, Design and Analysis". In: *ERCOFTAC international symposium 'Unsteady separation in fluid-structure'*. Mykonos, Greece.
- Rajappa, S., M. Ryll, H. H. Bühlhoff, and A. Franchi (2015). "Modeling, Control and Design Optimization for a Fully-actuated Hexarotor Aerial Vehicle with Tilted Propellers". In: *2015 IEEE Int. Conf. on Robotics and Automation*. Seattle, WA, pp. 4006–4013.
- Ramp, M. and E. Papadopoulos (2015). "On modeling and control of a holonomic vectoring tricopter". In: *2015 IEEE/RSJ Int. Conf. on Intelligent Robots and Systems*. Hamburg, Germany, pp. 662–668.
- Rashad, R., J. B. Engelen, and S. Stramigioli (2019). "Energy tank-based wrench/impedance control of a fully-actuated hexarotor: A geometric port-hamiltonian approach". In: *2019 IEEE Int. Conf. on Robotics and Automation*. Montreal, Canada, pp. 6418–6424.
- Rashad, R., P. Kuipers, J. Engelen, and S. Stramigioli (2017). "Design, Modeling, and Geometric Control on SE (3) of a Fully-Actuated Hexarotor for Aerial Interaction". In: *arXiv preprint arXiv:1709.05398*.
- Romero, H., S. Salazar, A. Sanchez, and R. Lozano (2007). "A new UAV configuration having eight rotors: Dynamical model and real-time control". In: *2007 46th IEEE Conference on Decision and Control*. New Orleans, LA, USA, pp. 6418–6423.
- Rongier, P., E. Lavarec, and F. Pierrot (2005). "Kinematic and dynamic modeling and control of a 3-rotor aircraft". In: *2005 IEEE Int. Conf. on Robotics and Automation*. Barcelona, Spain, pp. 2606–2611.
- Ryll, M., D. Bicego, and A. Franchi (2016). "Modeling and Control of FAST-Hex: a Fully-Actuated by Synchronized-Tilting Hexarotor". In: *2016 IEEE/RSJ Int. Conf. on Intelligent Robots and Systems*. Daejeon, South Korea, pp. 1689–1694.
- Ryll, M., H. H. Bühlhoff, and P. R. Giordano (2012). "Modeling and control of a quadrotor UAV with tilting propellers". In: *2012 IEEE Int. Conf. on Robotics and Automation*. Paul, MN, USA, pp. 4606–4613.
- (2013). "First flight tests for a quadrotor UAV with tilting propellers". In: *2013 IEEE Int. Conf. on Robotics and Automation*. Karlsruhe, Germany, pp. 295–302.
- (2015). "A novel overactuated quadrotor unmanned aerial vehicle: Modeling, control, and experimental validation". In: *IEEE Trans. on Control Systems Technology* 23.2, pp. 540–556.
- Ryll, M., G. Muscio, F. Pierri, E. Cataldi, G. Antonelli, F. Caccavale, and A. Franchi (2017). "6D Physical Interaction with a Fully Actuated Aerial Robot". In: *2017 IEEE Int. Conf. on Robotics and Automation*. Singapore, pp. 5190–5195.
- Saeed, A. S., A. B. Younes, S. Islam, J. Dias, L. Seneviratne, and G. Cai (2015). "A review on the platform design, dynamic modeling and control of hybrid UAVs". In: *2015 Int. Conf. on Unmanned Aircraft Systems*. Denver, CO, USA, pp. 806–815.
- Salazar-Cruz, S. and R. Lozano (2005). "Stabilization and nonlinear control for a novel trirotor mini-aircraft". In: *2005 IEEE Int. Conf. on Robotics and Automation*. Barcelona, Spain, pp. 2612–2617.

- Salazar-Cruz, S., R. Lozano, and J. Escareño (2009). “Stabilization and nonlinear control for a novel trirotor mini-aircraft”. In: *Control Engineering Practice* 17.8, pp. 886–894.
- Sanchez, A., J. Escareno, O. Garcia, and R. Lozano (2008). “Autonomous hovering of a noncyclic tiltrotor UAV: Modeling, control and implementation”. In: *IFAC Proceedings Volumes* 41.2, pp. 803–808.
- Sarkisov, Y., M. J. Kim, D. Bicego, D. Tsetserukou, C. Ott, A. Franchi, and K. Kondak (2019). “Development of SAM: cable-Suspended Aerial Manipulator”. In: *2019 IEEE Int. Conf. on Robotics and Automation*. Montreal, Canada.
- Scholz, G., M. Popp, J. Ruppelt, and G. F. Trommer (2016). “Model independent control of a quadrotor with tilttable rotors”. In: *2016 IEEE/ION Position, Location and Navigation Symposium (PLANS)*. Savannah, Georgia, USA, pp. 747–756.
- Segui-Gasco, P., Y. Al-Rihani, H. S. Shin, and A. Savvaris (2014). “A novel actuation concept for a multi rotor UAV”. In: *Journal of Intelligent & Robotics Systems* 74.1-2, pp. 173–191.
- Şenkul, F. and E. Altuğ (2013). “Modeling and control of a novel tilt—Roll rotor quadrotor UAV”. In: *2013 Int. Conf. on Unmanned Aircraft Systems*. Atlanta, USA, pp. 1071–1076.
- (2014). “Adaptive control of a tilt-roll rotor quadrotor UAV”. In: *2014 Int. Conf. on Unmanned Aircraft Systems*. Orlando, FL, USA, pp. 1132–1137.
- Servais, É., B. d’Andréa-Novel, and H. Mounier (2015). “Ground control of a hybrid tricopter”. In: *2015 Int. Conf. on Unmanned Aircraft Systems*. Denver, CO, USA, pp. 945–950.
- Servais, É., H. Mounier, and B. d’Andréa-Novel (2015). “Trajectory tracking of trirotor UAV with pendulum load”. In: *2015 20th International Conference on Methods and Models in Automation and Robotics (MMAR)*. Międzyzdroje, Poland, pp. 517–522.
- S.-Guerrero, D. and J. G. R.-Torres (2018). “The Hexapodopter: A Hybrid Flying Hexapod—Holonomic Flying Analysis”. In: *Journal of Mechanisms and Robotics* 10.5, pp. 1–1.
- Staub, N., D. Bicego, Q. Sablé, V. Arellano-Quintana, S. Mishra, and A. Franchi (2018). “Towards a Flying Assistant Paradigm: the OTHex”. In: *2018 IEEE Int. Conf. on Robotics and Automation*. Brisbane, Australia, pp. 6997–7002.
- Tadokoro, Y., T. Ibuki, and M. Sampei (2017). “Maneuverability analysis of a fully-actuated hexrotor UAV considering tilt angles and arrangement of rotors”. In: *IFAC-PapersOnLine* 50.1, pp. 8981–8986.
- Tognon, M. and A. Franchi (2018). “Omnidirectional Aerial Vehicles with Unidirectional Thrusters: Theory, Optimal Design, and Control”. In: *IEEE Robotics and Automation Letters* 3.3, pp. 2277–2282.
- Waslander, S. and C. Wang (2009). “Wind disturbance estimation and rejection for quadrotor position control”. In: *AIAA Infotech@ Aerospace conference and AIAA unmanned... Unlimited conference*, p. 1983.
- Yih, C. C. (2016). “Flight control of a tilt-rotor quadcopter via sliding mode”. In: *2016 International Automatic Control Conference (CAC)*. Taichung, Taiwan, pp. 65–70.
- Yoon, S., S. J. Lee, B. Lee, C. J. Kim, Y. J. Lee, and S. Sung (2013). “Design and flight test of a small tri-rotor unmanned vehicle with a LQR based onboard attitude control system”. In: *International Journal of Innovative Computing, Information and Control* 9.6, pp. 2347–2360.
- Yoshikawa, T. (1985). “Manipulability of robotic mechanisms”. In: *The International Journal of Robotics Research* 4.2, pp. 3–9.
- Young, Warren R (1982). *The Helicopters: The Epic of Flight*. Time-Life Books.
- Zhang, W., M. W. Mueller, and R. D’Andréa (2016). “A controllable flying vehicle with a single moving part”. In: *2016 IEEE Int. Conf. on Robotics and Automation*. Stockholm, Sweden, pp. 3275–3281.
- Zhao, M., K. Kawasaki, X. Chen, S. Noda, K. Okada, and M. Inaba (2017). “Whole-body aerial manipulation by transformable multirotor with two-dimensional multilinks”. In: *2017 IEEE Int. Conf. on Robotics and Automation*. Singapore, pp. 5175–5182.